NTIA Report 00-372

Indoor Polarization and Directivity Measurements at 5.8 GHz

Michael G. Cotton
Robert J. Achatz
Yeh Lo
Christopher L. Holloway

U.S. DEPARTMENT OF COMMERCE
William M. Daley, Secretary

Gregory L. Rohde, Assistant Secretary
for Communications and Information

November 1999

This Page Intentionally Left Blank

This Page Intentionally Left Blank

CONTENTS

This Page Intentionally Left Blank

This Page Intentionally Left Blank

INDOOR POLARIZATION AND DIRECTIVITY MEASUREMENTS AT 5.8 GHz

Michael G. Cotton, Robert J. Achatz, Yeh Lo, Christopher L. Holloway*

This report investigates how antenna polarization and directivity affect indoor radio channel bandwidth and signal coverage. Indoor impulse response measurements were taken at 5.8 GHz for four canonical propagation conditions: within a room, down a corridor, from a corridor into a room, and around a corridor corner. Directional linearly-polarized (LP), directional circularly-polarized (CP), and omnidirectional LP antennas were employed, and conclusions were drawn from basic transmission loss, rms delay spread, and cross-polarization discrimination results. Measurements indicated less LP basic transmission loss than CP basic transmission loss for both line-of-sight (LOS) and obstructed (OBS) channels. Also, LP rms delay spread was similar to CP rms delay spread in both LOS and OBS paths. The apparent advantage of using LP signals over CP signals indoors may be attributed to the relatively high degree of circular depolarization measured. Results also supported the use of omnidirectional antennas indoors to improve signal coverage. Omnidirectional measurements, however, demonstrated large delay spreads for some extraneous cases. These cases are emphasized to demonstrate the potential diversity holds for improving bandwidth capacity of indoor communication systems.

Key words: complex impulse response measurements; indoor propagation; polarization; delay spread; basic transmission loss; cross-polarization discrimination; antenna directivity

1. INTRODUCTION

In this study, we examined how polarization and directivity affect bandwidth and coverage limitations of indoor-propagation channels at 5.8 GHz. This frequency band was chosen due to the emergence of the NII WLAN [1]. Similar experiments have been performed at 1.3 and 4.0 GHz [2], at 5 GHz [3], and at 5.3 GHz [4]. Observations were based on wideband impulse response measurements using three antenna types (i.e., directional LP, directional CP, and omnidirectional LP) in four canonical propagation conditions: in-room, in-corridor, corridor-corner, and corridor-to-room (see Figure 1, Tables 1 and 2). System specification and measurement procedure, indoor channel specification, and data analysis techniques are described in Sections 2, 3, and 4 respectively.

We focused on co-polar transmission in order to observe advantages and disadvantages in transmitting LP versus CP signals. It was conjectured in [2] that directional CP antennas are more likely to reduce rms delay spread when compared to directional and omnidirectional LP antennas in

*The authors are with the Institute for Telecommunication Sciences, National Telecommunications and Information Administration, U.S. Department of Commerce, Boulder, CO 80303.

Table 1. Site Descriptions

	Site 1	Site 2	Site 3	Site 4	Site 5
Description	in-room	in-corridor	in-corridor	corridor-corner	corridor-to-room
Link type	LOS	LOS	LOS	OBS	OBS
$d_{T\text{-}R}$ [m]	5.0 - 6.8	12.2 - 14.0	45.7 - 47.5	8.3 - 10.1	13.7 - 15.5
ψ [degrees]	180.0	180.0	180.0	90.0	152.8

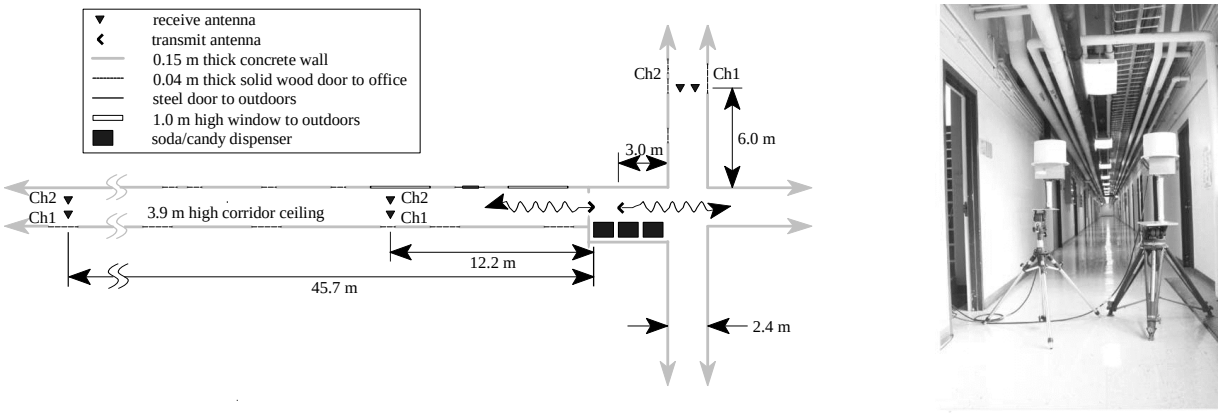

(a) (b)

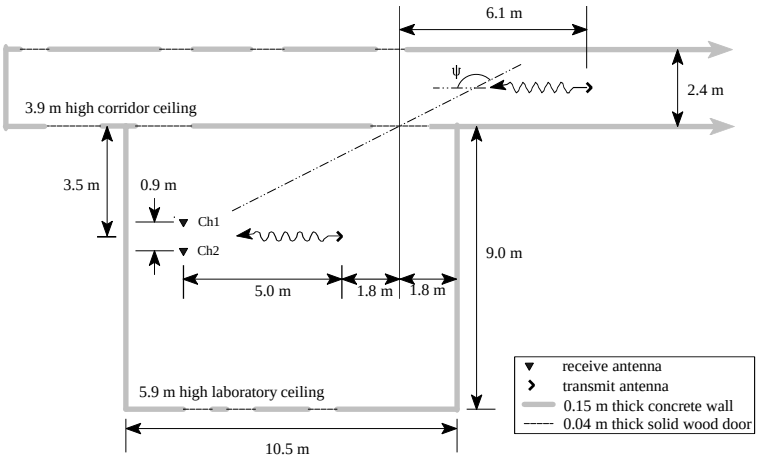

(c)

Figure 1. Measured indoor channel geometries: (a) in-corridor and corridor-corner scenarios, (b) receive antennas in corridor, (c) in-room and corridor-to-room scenarios.

Table 2. Antenna Configurations with Corresponding Nominal Gains and 3-dB Beamwidths

Antenna configuration	T_x antenna	Gain [dBi]	Beam width	Channel 1 R_x antenna	Gain [dBi]	Beam width	Channel 2 R_x antenna	Gain [dBi]	Beam width
CBAS - CBAS (1a)	LH-CBAS	6.7	60°	RH-CBAS	6.7	60°	LH-CBAS	6.7	60°
CBAS - CBAS (1b)	LH-CBAS	6.7	60°	LH-CBAS	6.7	60°	RH-CBAS	6.7	60°
CBAS - OMNI (2)	LH-CBAS	6.7	60°	V-OMNI	1.0	360°	V-OMNI	1.0	360°
CBAS - DLPLP (3)	LH-CBAS	6.7	60°	V-DLPLP	6.1	60°	H-DLPLP	6.1	60°
LPLP - CBAS (4a)	V-LPLP	6.5	60°	RH-CBAS	6.7	60°	LH-CBAS	6.7	60°
LPLP - CBAS (4b)	V-LPLP	6.5	60°	LH-CBAS	6.7	60°	RH-CBAS	6.7	60°
LPLP - OMNI (5)	V-LPLP	6.5	60°	V-OMNI	1.0	360°	V-OMNI	1.0	360°
LPLP - DLPLP (6)	V-LPLP	6.5	60°	V-DLPLP	6.1	60°	H-DLPLP	6.1	60°
OMNI - CBAS (7a)	V-OMNI	1.0	360°	RH-CBAS	6.7	60°	LH-CBAS	6.7	60°
OMNI - CBAS (7b)	V-OMNI	1.0	360°	LH-CBAS	6.7	60°	RH-CBAS	6.7	60°
OMNI - OMNI (8)	V-OMNI	1.0	360°	V-OMNI	1.0	360°	V-OMNI	1.0	360°
OMNI - DLPLP (9)	V-OMNI	1.0	360°	V-DLPLP	6.1	60°	H-DLPLP	6.1	60°

LOS paths. In support, we know that the tangential electric field component of an incident radio wave will be shifted in phase by 180 degrees when reflected off a metallic surface, while the normal electric field component will not be shifted. Therefore, a CP signal reflected off a metallic surface changes to the opposite polarization while a LP signal remains the same. This suggests that CP signals would have smaller delay spread and more basic transmission loss than LP signals, since only signals with an odd number of bounces will be received.

The assumed advantage of CP signals to reduce delay spread requires the propagation channel to have low depolarization characteristics. Most building surfaces and obstructions, however, have lossy-dielectric properties, corners, and other features which depolarize the signal. Thus, it is necessary to quantify the effects of depolarization on delay spread and basic transmission loss to determine the effectiveness of CP signals compared to LP signals. The dual-channel receiver allowed us to simultaneously digitize the cross-polarization signal, compute the cross-polarization discrimination, and determine the amount of depolarization at each site.

We also investigated the influence of antenna directivity indoors. Directivity can allow an antenna to radiate or receive more effectively. If the optimal orientation of the antenna is known (as in LOS cases), then delay spread can be reduced by maximizing the gain in the optimal direction (as demonstrated in Figure 2). LOS paths, however, are not always available indoors; portable (e.g., laptops) and mobile (e.g., electronic clipboards) units are examples of WLAN applications where OBS paths are readily encountered. Obstructions cause the effective radiation pattern to be distorted, and without a smart antenna to optimally steer the beam, the benefit of directivity is in question.

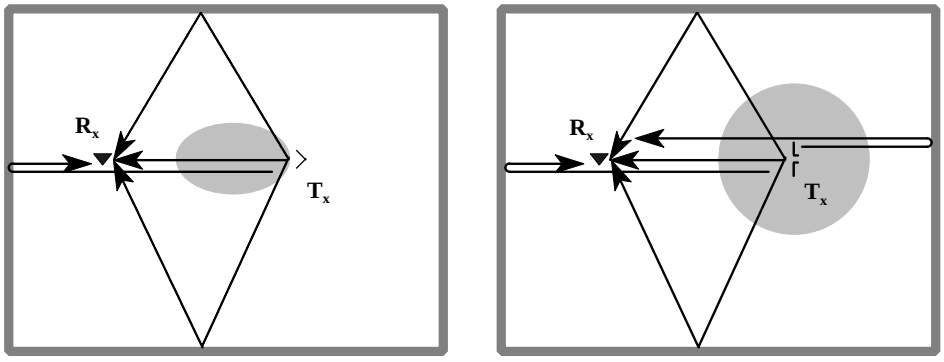

(a) (b)

Figure 2. First-order rays arriving at a receiver for (a) directional and (b) OMNI transmit antennas. Shaded areas represent transmit antenna patterns.

Measurements were conducted at sites chosen to give a broad representation of the propagation mechanisms of a typical indoor environment.

In this report, we have disregarded specific questions concerning diversity, such as those analyzed in [5]; results, however, are displayed to provide examples where diversity would improve the coverage and bandwidth capacities of the communication system. Bit-error-rate computation is also beyond the scope of this report. Delay spread and basic transmission loss results are compared quantitatively in order to draw conclusions on the effects of polarization and directivity. An in-depth discussion of the results is provided in Section 5 and summarized in Section 6.

2. MEASUREMENT SYSTEM AND PROCEDURE

The wideband digital sampling probe, developed at ITS and utilized in this experiment, is comprised of a transmitter and a dual channel receiver [6, 7]. The transmitter uses a 250-Mb/sec 127-bit maximal length pseudo-random noise (PN) code to BPSK modulate a 5.8-GHz RF carrier. This signal is bandpass-filtered, amplified, and fed into the transmit antenna. A step attenuator is used to control the signal power delivered to the transmit antenna in order to achieve reasonable signal-to-noise ratios for each independent measurement. The received signal, modified by the radio channel, is down-converted to an intermediate frequency (IF) and digitized at 4 samples per chip or 1 GS/s. A personal computer is used to control the measurement system receiver. After the signal is digitized by the oscilloscope, the IF signal is transferred over the GPIB bus to the computer. Next, the signal is down-converted to baseband via software, and the complex impulse response is computed by cross-correlating the discrete baseband signal with a copy of the PN code. Block diagrams for the transmitter and receiver modules are shown in Figures 3 and 4 with component descriptions given in Appendix C.

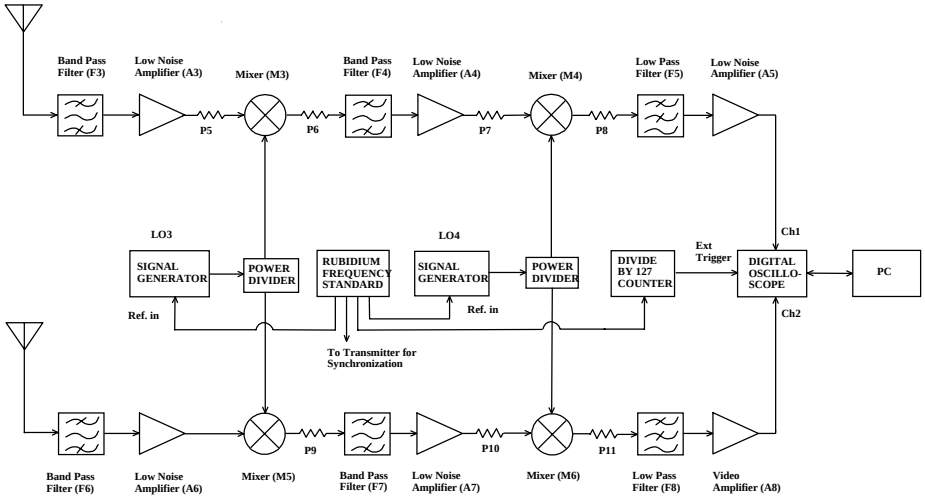

Figure 3. Receiver block diagram.

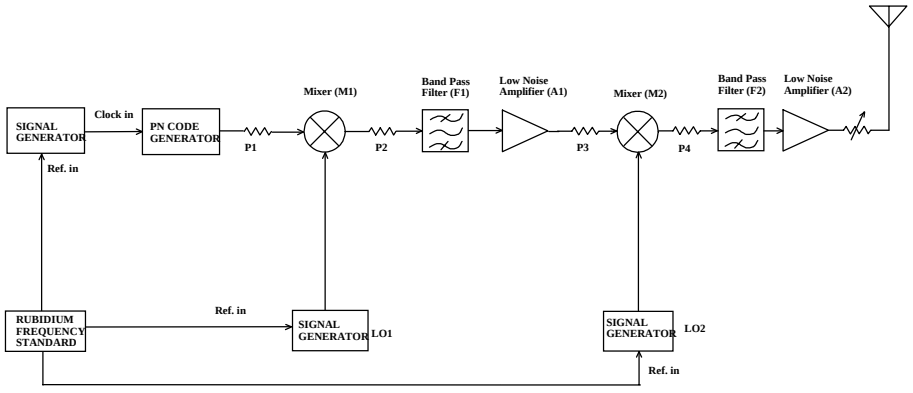

Figure 4. Transmitter block diagram.

Back-to-back calibration, system verification, and setup procedure were performed daily to make sure the system operated properly before the actual measurements began. The noise figure of the receiving system was found to be 7 dB and 11 dB for channels 1 and 2, respectively. Examples of impulse responses captured during calibration are given in Figure 5. Notice that the smallest measurable delay spread is 1.3 ns and the maximum interval of discrimination (*IOD*) is 38.4 dB, where the acronym *IOD* quantifies the maximum interval between the peak of the power delay profile and the processing noise floor. Theoretical *IOD* for a 127-bit maximum-length PN code is 42.1 dB. The chip rate of the PN code generator allows a time delay resolution of 4 ns or 1.2 meters in a spatial sense, and the maximum delay is 508 ns which corresponds to approximately 154 m for a radio wave traveling at the speed of light.

Nine transmit- and receive-antenna combinations were used for this experiment (see Table 2). Antenna calibrations were performed in an anechoic chamber to confirm manufacturer specifications and measure co- and cross-polarization gains. All directional antennas have approximately a 60-degree 3-dB beamwidth. The following abbreviations are used: left-hand circular (LH), right-hand circular (RH), vertical linear (V), horizontal linear (H), cavity-backed Archimedes spiral antenna (CBAS), linear-polarized log periodic antenna (LPLP), dual-linear-polarized log periodic antenna (DLPLP), and linearly-polarized omnidirectional antenna (OMNI).

Measurements were made during non-working hours so that there would be no people walking within the measurement area to influence the results. For each measurement site, the receiver was kept stationary and the transmitter, mounted on a cart, was moved back and forth along a 1.8-m (40λ) linear path at approximately 0.3 m/s. The time between impulses was 15 ms; hence, an impulse was recorded about every 0.1λ along the path. A single measurement consisted of three bursts of 128 impulse responses. The dual channel receiver was held in an equipment rack with two receiving antennas mounted on tripods 1.2 m above the ground and at 17 wavelengths separation.

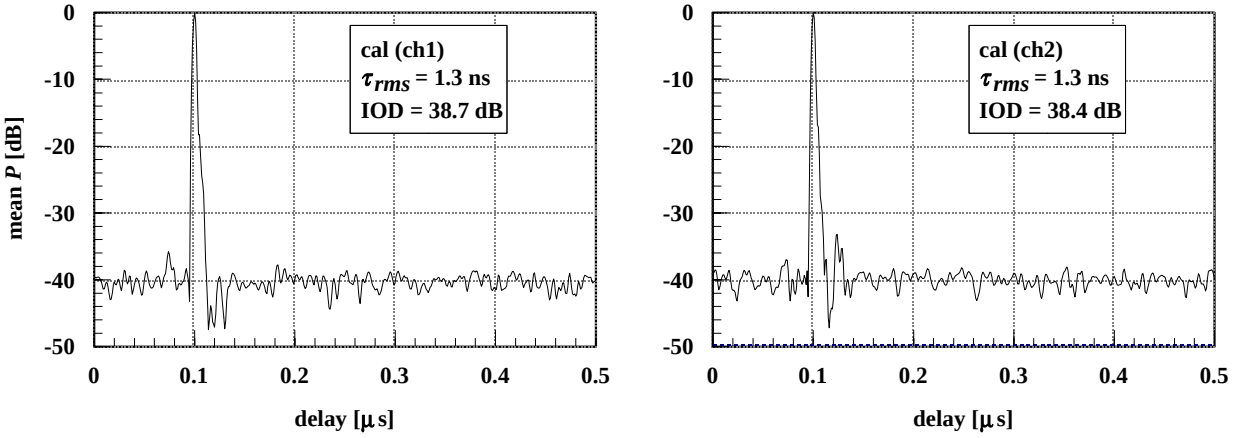

Figure 5. Examples of calibration mean power delay profiles.

3. MEASURED INDOOR CHANNEL SPECIFICATION

Complex impulse response measurements were made inside the U.S. Department of Commerce Radio Building in Boulder, Colorado using the digital sampling channel probe described previously. The Radio Building is supported by poured concrete columns and cinder block interior and exterior walls. Presumably, rebar exists in the exterior walls and columns. The four cases (in-room, in-corridor, corridor-corner, and corridor-to-room) were encompassed by five measurement sites: 1) LOS in-room, 2) LOS in-corridor with ~13.3-m T-R separation, 3) LOS in-corridor with ~46.6-m T-R separation, 4) OBS corridor-corner, and 5) OBS corridor-to-room. The sites are presented in Figure 1, summarized in Table 1, and described in detail in the following sections. Antenna orientation was quantified by the angle ψ between transmit and receive boresight direction vectors. Also, $d_{T\text{-}R}$ is the transmitter-receiver (T-R) separation which varies by ±0.9 m.

3.1. In-room case

Site 1 was within a 9.0-m-long, 10.5-m-wide, 5.9-m-high empty laboratory. The lab is bounded by interior concrete walls and accessed by solid wood doors. Adjacent to the laboratory is a corridor, laboratories of comparable size on either side, and three offices on the opposite side of the lab from the corridor. The roof structure includes windows along the entire length of the lab. A LOS link was established by placing the receiver and transmitter near the center of the lab. The separation distance ranged from 5.0 to 6.8 m as the transmitter moved along a 1.8-m track during acquisitions. The receive antennas were mounted directly facing the transmit antenna.

3.2. In-corridor case

Sites 2 and 3 were within a 2.4-m-wide, 3.9-m-high concrete corridor. The corridor is over 100 m long which gives it a large geometric aspect ratio (i.e., ratio of maximum dimension to minimum dimension). The corridor is linked to adjacent offices and laboratories via solid wood doors and to the outdoors via windows and steel doors. Above 2.1 m, a complex scattering environment exists due to numerous pipes, vents, and network cables in the ceiling (see Figure 1b). T-R separation ranged from 12.2 m to 14.0 m for site 2 and from 45.7 m to 47.5 m for site 3. For both sites, a LOS path was present and the receive and transmit antennas directly faced each other.

3.3. Corridor-corner case

In an attempt to isolate the effects of diffraction we measured the impulse response around a corridor corner. In this case (site 4), we assumed the diffraction path was stronger than the direct path through the corner. Hence, the antenna orientation was chosen such that the antennas faced directly down their respective orthogonal corridors. T-R separation ranged from 8.3 m to 10.1 m. Notice the location of the highly conductive soda/candy dispensers.

3.4. Corridor-to-room case

The corridor-to-room case (site 5) was a combination of the in-room and in-corridor cases, but the line-of-sight was obstructed. The transmit antenna was pointing directly down the corridor (approximately 11° from being directed at the door). It should be noted that the open door leading to the room was well within the main beam of the transmit antenna. The receive antennas, inside the empty laboratory, were pointed directly at the adjoining open doorway assuming the strongest path passed through it. T-R separation was 13.7 - 15.5 m.

4. DATA ANALYSIS

Basic transmission loss data and delay statistics indicate coverage and data rate limitations, respectively. Cross-polarization discrimination provides information about depolarization characteristics of the measured channel. This section presents a detailed explanation of the data analysis used in this report.

The formulation of basic transmission loss and delay statistics begins with the power delay profile (PDP), given by

$$P_n(\tau_m) = \Re[h_n(\tau_m)]^2 + \Im[h_n(\tau_m)]^2 \quad , \qquad \textbf{(1)}$$

where $h(n, \tau_m)$ is a measured complex impulse response, τ_m is the delay of the m^{th} sample, and n is the impulse index. Received power of the n^{th} impulse is the sum of the powers over all delays or

$$P_{R,n} = \sum_{m=1}^{M} P_n(\tau_m) \quad , \qquad \textbf{(2)}$$

where M is the number of samples per impulse. The mean power delay profile is formulated as

$$\overline{P}(\tau_m) = \frac{1}{N} \sum_{n=1}^{N} P_n(\tau_m) \quad , \qquad \textbf{(3)}$$

where N (= 384) is the total number of impulses acquired. Averaging the impulses smooths out the noise floor and allows for a determination of *IOD*, which is again defined as the maximum interval between the peak of the power delay profile and the processing noise floor.

Historically, GWSUS (Gaussian, Wide-sense Stationary, Uncorrelated Scattering) channels were assumed and rms delay spread was used to estimate bit-error rates for digitally modulated signals [8-

10]. The Gaussian nature of the indoor impulse responses (or Rayleigh nature since *h* is complex), however, is in question. In fact, a brief investigation of the distributions of amplitudes at specific delays showed a non-Rayleigh behavior in LOS cases and antenna combinations using directional antennas. Hence, the mean power delay profile may not represent a spatially averaged PDP that characterizes the location as in [9] and therefore should not be used to predict the bit error rate of radios operating in GWSUS channels as described in [10]. A communications engineer might question the integrity of the term "rms delay spread" if the GWSUS assumption is not met; but for the purpose of this report, measures are only needed for a qualitative assessment of intersymbol interference (ISI) and the term is maintained as a blind mathematical function for the sake of simplicity and comparison.

4.1. Delay spread

Time-dispersive indoor propagation channels cause intersymbol interference at high data rates. The parameter used to quantify ISI has been rms delay spread [10], which is defined as the square root of the second central moment of the mean PDP, given as

$$\tau_{rms,(a)} = \sqrt{\frac{\sum_{m=1}^{M} (\tau_m - \bar{\tau})^2 \bar{P}(\tau_m)}{\sum_{m=1}^{M} \bar{P}(\tau_m)}} \quad . \qquad \textbf{(4)}$$

In this equation the *(a)* subscript denotes antenna configuration and $\bar{\tau}$ is the first moment or mean delay of the mean PDP, given by

$$\bar{\tau} = \frac{\sum_{m=1}^{M} \tau_m \bar{P}(\tau_m)}{\sum_{m=1}^{M} \bar{P}(\tau_m)} \quad , \qquad \textbf{(5)}$$

where *M* is the number of samples per impulse. Values 20 dB or more below the peak of the mean PDP were set to zero so noise would not influence delay statistics. Another relevant quantity is the delay spread of a single PDP which is displayed in the scatter plots in Appendix A.

4.2. Basic transmission loss

Given the measurement conditions, received power may be attenuated for a number of reasons (e.g., channel effects, polarization mismatch, antenna pattern effects, etc.). Inclusion of all site- and

antenna-dependent sources of loss is preferable in order not to impose inaccurate assumptions, such as optimal antenna orientation or polarization match. Since basic transmission loss does not account for angular or polarization dependency it was chosen to quantify loss. It is computed from the average power received over the ensemble of impulses in the 1.8-m track and given by

$$L_{(a)} = \frac{P_T G_T G_R}{\frac{1}{N}\sum_{n=1}^{N} P_{R,n}} \quad , \tag{6}$$

where P_T is the transmitted power, G_T and G_R are the nominal gains for the transmit and receive antennas (see Table 2), and the subscript *(a)* denotes antenna configuration. Another relevant quantity is the basic transmission loss of a single impulse, given as

$$\ell_n = \frac{P_T G_T G_R}{P_{R,n}} \quad , \tag{7}$$

which is displayed in the scatter plots in Appendix A.

4.3. Cross-polarization discrimination

Cross-polarization discrimination (*XPD*) is formulated as

$$XPD_{(a)} = \frac{\sum_{m=1}^{M} \overline{P_C}(\tau_m)}{\sum_{m=1}^{M} \overline{P_X}(\tau_m)} \quad , \tag{8}$$

where the subscript *C* stands for co-polar and *X* stands for cross-polar. *XPD* quantifies depolarization characteristics of a channel. In a non-depolarizing environment (e.g., anechoic chamber) the co-polar signal will remain strong relative to the cross-polar signal, and *XPD* will be large. As the degree of depolarization grows, the polarization plane of the signal at the receiver rotates and the *XPD* decreases. Therefore, small *XPD* or a significant reduction in *XPD* from that measured in a non-depolarizing channel is attributed to a high degree of depolarization.

5. RESULTS

The four cases (in-room, in-corridor, corridor-corner, and corridor-to-room) were encompassed by five measurement sites summarized in Table 1. For each impulse, basic transmission loss and delay

spread were computed and presented in scatter plots in Appendix A. Although delay spread of a single PDP means little to the communications engineer, who historically relates ISI to rms delay spread, these plotted pairs are provided to add some insight to the distribution of such parameters and are frequently referred to in the current discussion. From the complex impulse response data, rms delay spreads and basic transmission loss were computed and tabulated in Table 3. Mean PDPs and corresponding 20-dB thresholds are plotted in Appendix B.

Table 3. Basic Transmission Loss and RMS Delay Spread

Antenna configuration	In-room (site 1)		In-corr. (site 2)		In-corr. (site 3)		Corr.-corner (site 4)		Corr.-to-rm. (site 5)		measure [units]
	ch1	ch2	ch1	ch2	ch1	ch2	ch1	ch2	ch1	ch2	
CBAS - CBAS	75.0	64.5	73.7	70.7	82.0	77.3	84.2	84.7	81.6	84.7	$L_{(1a)}$ [dB]
(1a)	12.6	2.3	3.0	3.2	2.5	2.5	12.4	12.0	3.2	11.5	$\tau_{rms,(1a)}$ [ns]
CBAS - CBAS	65.2	75.2	72.2	70.5	75.2	81.6	83.8	84.7	84.3	80.7	$L_{(1b)}$ [dB]
(1b)	2.1	11.2	3.6	3.3	3.0	3.3	13.4	11.5	7.5	3.0	$\tau_{rms,(1b)}$ [ns]
CBAS - OMNI	64.3	64.0	68.2	65.9	73.7	75.9	80.6	80.4	78.4	76.5	$L_{(2)}$ [dB]
(2)	6.4	5.5	5.5	8.1	3.4	104.0	15.2	9.4	8.9	4.6	$\tau_{rms,(2)}$ [ns]
CBAS - DLPLP	61.8	64.3	70.0	69.6	72.1	75.9	80.7	82.3	79.1	80.0	$L_{(3)}$ [dB]
(3)	1.5	1.7	3.4	3.4	3.2	3.0	13.4	12.3	3.4	3.8	$\tau_{rms,(3)}$ [ns]
LPLP - CBAS	66.0	65.5	71.4	70.1	73.9	79.5	82.6	84.3	83.2	81.9	$L_{(4a)}$ [dB]
(4a)	1.8	1.6	3.7	3.5	3.1	3.5	11.8	11.1	8.2	3.4	$\tau_{rms,(4a)}$ [ns]
LPLP - CBAS	65.0	66.5	69.8	71.9	74.1	73.1	83.2	83.3	86.2	81.7	$L_{(4b)}$ [dB]
(4b)	2.4	1.9	3.8	3.9	2.0	2.2	11.1	10.0	17.6	9.8	$\tau_{rms,(4b)}$ [ns]
LPLP - OMNI	62.2	60.2	64.2	65.5	69.1	70.7	79.0	79.5	77.3	74.4	$L_{(5)}$ [dB]
(5)	8.2	4.9	4.0	8.5	2.1	24.7	12.1	8.9	13.5	3.8	$\tau_{rms,(5)}$ [ns]
LPLP - DLPLP	61.5	80.5	65.9	76.3	67.2	81.4	80.1	86.4	79.4	84.5	$L_{(6)}$ [dB]
(6)	1.4	18.3	3.5	5.4	2.8	3.8	13.5	12.3	4.0	4.8	$\tau_{rms,(6)}$ [ns]
OMNI - CBAS	64.2	63.8	67.0	69.7	69.1	73.4	80.3	81.5	79.9	75.7	$L_{(7a)}$ [dB]
(7a)	7.9	7.3	3.6	14.9	2.5	2.8	16.3	12.8	7.0	3.1	$\tau_{rms,(7a)}$ [ns]
OMNI - CBAS	63.4	65.1	67.0	66.8	72.2	72.0	79.9	80.8	80.0	74.9	$L_{(7b)}$ [dB]
(7b)	8.1	8.1	3.2	9.0	2.9	3.3	15.7	10.8	6.1	3.8	$\tau_{rms,(7b)}$ [ns]
OMNI - OMNI	n/a	58.2	62.9	n/a	69.8	n/a	n/a	75.3	69.8	n/a	$L_{(8)}$ [dB]
(8)	n/a	9.9	4.6	n/a	2.9	n/a	n/a	10.0	3.6	n/a	$\tau_{rms,(8)}$ [ns]
OMNI - DLPLP	58.9	75.1	62.2	70.4	67.6	75.1	75.3	84.1	70.6	82.8	$L_{(9)}$ [dB]
(9)	6.3	20.3	3.2	5.6	2.6	2.6	15.9	13.5	4.0	7.7	$\tau_{rms,(9)}$ [ns]

We are interested in how directional LP, directional CP, and omnidirectional LP antennas interact in a "mixed" system. These scenarios may arise for proprietary or economical reasons. Hence, we measured the channel impulse response for all nine possible transmit-receive antenna combinations. It is difficult, however, to draw many conclusions regarding mixed systems. In short, no significant disadvantage was observed when mixed systems were deployed (i.e., most antenna combinations clump together in the scatter plots). Henceforth, the mixed system scenarios are disregarded for a more comprehensive and focused representation of the results.

In the following two sections, effects of polarization and directivity within a depolarizing indoor channel are analyzed. Toward this end, we focus on co-polarized transmission and its relation to *XPD*. Results in Table 3 are difficult to compare between sites; therefore, we normalized basic transmission loss and rms delay spread to the OMNI-OMNI results within each site. Antenna configuration subscripts in the formulation of $L_{(a)}$, $J_{rms,(a)}$, and $XPD_{(a)}$ were used to clarify this normalization in the presentation of results given in Table 4 and Figure 6.

5.1. Polarization analysis

In this section, combinations with directional-receive and directional-transmit antennas (i.e., combinations 1 and 6) are considered in order to isolate polarization from directivity results. Under these constraints, we assume variation in results were due to polarization mismatch because free-space loss and loss due to angular dependency at each site were constant. That is, we assume T-R separation is constant, R is constant, and the channel is stationary.

A purpose of this study was to extend indoor measurement scenarios to highly depolarizing indoor channels. The range of depolarization encompassed by the measurements was quantified by the cross-polarization results given in Table 5. Anechoic chamber results showed that the circularly-polarized CBAS antennas used in this experiment were capable of measuring higher *XPD* than the linearly-polarized LPLP antennas. We attribute this to the CP antennas being less sensitive to alignment in the polarization plane. The *XPD* limitations posed by these antennas are sufficient for our purposes as shown by the low *XPD* measured at each site. Relative to the anechoic chamber results, a drastic reduction in *XPD* was measured with the CP antennas. Additionally, results reflected less CP *XPD* than LP *XPD* for both LOS and OBS paths. From these observations we deduce that CP signals were depolarized more than the LP signals in the indoor channels measured. The effects of depolarization on delay spread and basic transmission loss are shown in Figure 7. There is a trend where co-polar basic transmission loss and rms delay spread increase with decreasing *XPD*.

The theoretical justification behind the use of CP signals instead of LP signals, to reduce delay spread in LOS indoor channels, assumes insignificant depolarization. By comparing antenna combinations 1 and 6 in Table 4, one can observe that CP signals achieved lower delay spreads than LP signals in site 1. Results show, however, that transmitting within an empty room and receiving a short distance from the transmitter is an exception amongst scenarios considered in this report.

Table 4. Co-polar Results Normalized to OMNI-OMNI Results in Each Site

Antenna configuration	In-room (site 1)	In-corridor (site 2)	In-corridor (site 3)	Corridor-corner (site 4)	Corridor-to-room (site 5)	measure [units]
CBAS - CBAS	+6.3	+7.8	+7.5	+9.4	+14.9	$L_{(1a)}/L_{(8)}$[dB]
(1a)	-7.6	-1.4	-0.4	+2.0	+7.9	$\tau_{rms,(1a)} - \tau_{rms,(8)}$ [ns]
CBAS - CBAS	+7.0	+7.6	+5.4	+8.5	+14.5	$L_{(1b)}/L_{(8)}$ [dB]
(1b)	-7.8	-1.3	-0.1	+3.4	+3.9	$\tau_{rms,(1b)} - \tau_{rms,(8)}$ [ns]
LPLP - OMNI	+4.0, +2.0	+1.3, +2.6	-0.7, +0.9	+3.7, +4.2	+7.5, +4.6	$L_{(5)}/L_{(8)}$ [dB]
(5)	-1.7, -5.0	-0.6, +3.9	-0.8, +21.8	-1.1, 0.0	+9.9, +0.2	$\tau_{rms,(5)} - \tau_{rms,(8)}$ [ns]
LPLP - DLPLP	+3.3	+3.0	-2.6	+4.8	+9.6	$L_{(6)}/L_{(8)}$ [dB]
(6)	-8.5	-1.1	-0.1	+3.5	+0.4	$\tau_{rms,(6)} - \tau_{rms,(8)}$ [ns]
OMNI - OMNI	+0.0	+0.0	+0.0	+0.0	+0.0	$L_{(8)}/L_{(8)}$ [dB]
(8)	+0.0	+0.0	+0.0	+0.0	+0.0	$\tau_{rms,(8)} - \tau_{rms,(8)}$ [ns]
OMNI - DLPLP	+0.7	-0.7	-2.2	+0.0	+0.8	$L_{(9)}/L_{(8)}$ [dB]
(9)	-3.6	-1.4	-0.3	+5.9	+0.4	$\tau_{rms,(9)} - \tau_{rms,(8)}$ [ns]

Shaded blocks highlight the minimum (light grey) and maximum (dark grey) basic transmission loss at each site.

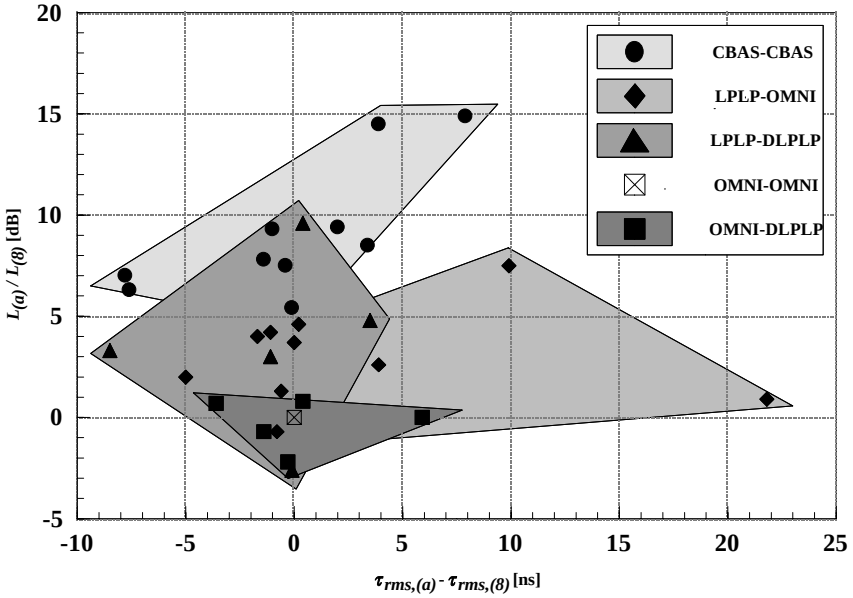

Figure 6. Co-polar basic transmission loss versus rms delay spread for five indoor sites. Data were normalized to OMNI-OMNI (8) results at each site.

Considering sites 2 - 5, CP and LP signals experience similar delay spreads for both LOS and OBS paths. In fact, we measured the worst co-polar performance (in terms of rms delay spread and basic transmission loss) with CP antennas. Results in [2] supported directional CP antennas to reduce rms delay spread over omnidirectional and directional LP antennas in LOS paths. In-room results (site 1) support this hypothesis; however, in-corridor results (sites 2 and 3) do not. Since these results do not support the use of CP signals to reduce delay spread in a general sense, indoor depolarization should not be considered negligible. In fact, we might go so far as to say that indoor depolarization is a dominant phenomenon, one which makes it difficult to choose a "best" polarization for indoor communications in terms of improving bandwidth capacity.

Basic transmission loss results show that CP signals experience greater loss than LP signals for both LOS and OBS paths (observe the shaded blocks in Table 4). This is expected because in the limiting case, where the reflecting surfaces are perfect conductors, there is no loss due to LP mismatch and significant loss due to CP mismatch (since only rays of even numbers of bounces are received). On the other hand, if the signals are completely depolarized then the excess loss due to polarization mismatch should be similar for the LP and CP signals. Between the limiting cases, loss due to CP mismatch exceeds loss due to LP mismatch (as measured).

Table 5. Circular and Linear Cross-polarization Discrimination

Antenna configuration	Anechoic chamber	In-room (site 1)	In-corridor (site 2)	In-corridor (site 3)	Corridor-corner (site 4)	Corridor-to-room (site 5)
CBAS-CBAS (1a)	+50.2	+10.5	+3.0	+4.7	-0.5	-3.1
CBAS-CBAS (1b)	+50.2	+10.0	-1.7	+6.4	+0.9	-3.6
LPLP-DLPLP (6)	+24.4	+19.0	+10.4	+14.2	+6.3	+5.1

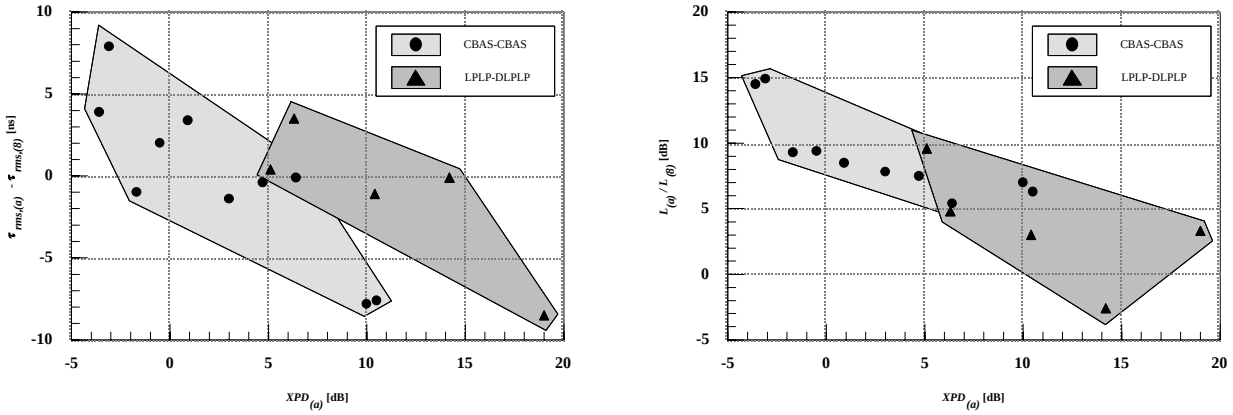

(a) (b)

Figure 7. Co-polar (a) rms delay spread and (b) basic transmission loss versus *XPD* at five indoor sites. Data were normalized to OMNI-OMNI (8) results at each site.

5.2. Directivity analysis

In this section we discuss the tradeoffs between OMNI versus directional antennas observed in the measurements. LP cases (combinations 5, 6, 8, and 9) are the focus of this section in order to isolate directivity from polarization results.

One might presume that a disadvantage of OMNI antennas is an increased probability of receiving large numbers of significant delayed rays, since all rays are radiated equally in all directions (see Figure 2). An example of the high delay spread from the use of OMNI antennas is demonstrated in Table 3 (site 3, ch2, antenna combination 5). For this case, mean PDP plots in Appendix B show a significant signal received approximately 380 ns after the direct path (most likely resulting from a single reflection off a far wall). This observation lends itself to the promotion of diversity to increase bandwidth capacity for extraneous cases since the same effect was not measured with the opposite channel. Large delay spreads due to the use of OMNI antennas are also apparent in the scatter plots in Appendix A, especially at sites where the geometric aspect ratio is large (e.g., site 3). Notice the high delay spreads corresponding to the V-OMNI receive antenna cases (square symbols) and the more subtle delay spread increase associated with transmit OMNI antennas by comparing Figure A-2 to Figure A-3.

Here we consider basic transmission loss as a metric for analyzing the effects of directivity in transmit antennas. For LOS paths, we measured similar basic transmission loss in omnidirectional (i.e., combinations 8 and 9) and directional (i.e., combinations 5 and 6) transmit antenna cases. OBS paths add a degree of uncertainty to the determination of the optimal antenna orientation. One might hypothesize that if the primary propagation paths are within the 3-dB beamwidth, then basic transmission loss results would be similar. OBS channel results, however, disagree with this hypothesis. To the best of our knowledge, antennas were aligned so that the primary propagation paths were within the main beam; yet, a significant decrease in power was received from directional-transmit antennas relative to OMNI-transmit antennas (e.g., 4 dB less for site 4 and 8 dB less for site 5). It seems high-order rays, which encounter large numbers of reflections and are likely to originate outside a directional antenna's main beam, contribute significantly to the signal received in OBS paths. In summary, OMNI transmit antennas are more effective in providing stronger signal coverage indoors at the risk of increased delay spread.

6. CONCLUSION

Dual-channel impulse response measurements were conducted in four canonical cases chosen to give a broad representation of typical indoor propagation channels at 5.8 GHz. The purpose was to expand indoor propagation measurements to scenarios of a high degree of depolarization and to observe basic transmission loss and delay spread behavior when signals were transmitted and received with a variety of antennas (i.e., polarization and directivity variation). Measurements supported the following results.

Delay spread results:

1. CP and LP signals have similar delay spreads for both LOS and OBS paths (see Figure 6).
2. Omnidirectional transmit and receive antennas (e.g., combinations 5, 8, and 9) produce higher delay spreads, especially for channels with large geometric aspect ratios (e.g., corridor).
3. Delay spread increases as the degree of depolarization increases (see Figure 7).

Basic transmission loss results:

4. CP signals have greater basic transmission loss than LP signals in both LOS and OBS paths (see Table 4).
5. OMNI transmit antennas provide stronger signal coverage than directional transmit antennas for OBS paths.
6. Basic transmission loss increases as the degree of depolarization increases (see Figure 7).

Depolarization results:

7. CP signals are depolarized more than LP signals (see Table 5).
8. The indoor channel significantly depolarizes transmitted signals.

When considering a broad representation of indoor scenarios (i.e., a wide range of depolarization), it does not appear that CP signals offer advantages over LP signals for co-polarized transmission. These findings are due to the strong depolarization characteristics of the indoor channel reflected in the *XPD* data. Results support the use of omnidirectional antennas indoors to improve signal coverage at the risk of increased delay spreads.

As mentioned in the text, we limited the scope of this work to co-polarized transmission with little regard to diversity. The large amount of depolarization variance evident in the CP case suggests that CP diversity may be better than LP diversity to improve coverage. If OMNI antennas were used, then diversity to minimize extraneous high delay spread cases should prove effective. Work is needed to determine if fading in the orthogonal channel is independent before we draw any conclusions.

7. ACKNOWLEDGMENTS

The authors would like to thank J. Randy Hoffman for the development of the measurement system and Peter B. Papazian and George A. Hufford for insights shared.

8. REFERENCES

[1] R.O. LaMaire, A. Krishna, P. Bhagwat, and J. Panian, "Wireless LANs and mobile networking standards and future directions," *IEEE Communications Magazine*, vol. 34, no. 8, pp. 86-94, Aug. 1996.

[2] T.S. Rappaport and D.A. Hawbaker, "Wide-band microwave propagation parameters using circular and linear polarized antennas for indoor wireless channels," *IEEE Transactions on Communications*, vol. 40, no. 2, pp. 240-245, Feb. 1992.

[3] J. Medbo, H. Hallenberg, and J.E. Berg, "Propagation characteristics at 5 GHz in typical radio-LAN scenarios," *in Proc. IEEE Vehicular Technology Conference*, Houston, TX, May 1999, pp. 185-189.

[4] J. Kivinen and P. Vainikainen, "Wideband propagation measurements in corridors at 5.3 GHz," *in Proc. IEEE International Symposium on Spread Spectrum Techniques and Applications*, Sun City, South Africa, Sep. 1998.

[5] R.J. Achatz, Y. Lo, and E.E. Pol, "Indoor direction diversity at 5.8 GHz," NTIA Report 98-351, Jul. 1998.

[6] R.H. Espeland, E.J. Violette, and K.C. Allen, "Millimeter wave wide-band diagnostic probe measurements at 30.3 GHz on an 11.8 km link," NTIA Tech. Memo. TM-83-95, Sep. 1983.

[7] P.B. Papazian, Y. Lo, E.E. Pol, M.P. Roadifer, T.G. Hoople, and R.J. Achatz, "Wideband propagation measurements for wireless indoor communication," NTIA Report 93-292, Jan. 1993.

[8] P.A. Bello and B.D. Nelin, "The effect of frequency selective fading on the binary error probabilities of incoherent and differentially coherent matched filter receivers," *IEEE Transactions on Communications Systems*, vol. CS-11, no. 2, pp. 170-185, Jun. 1963.

[9] D.M. Devasirvatham, "Multipath time delay spread in the digital portable radio environment," *IEEE Communications Magazine*, vol. 25, no. 6, pp. 13-21, Jun. 1987.

[10] J.C-I Chuang, "The effects of time delay spread on portable radio communications channels with digital modulation," *IEEE Journal on Selected Areas of Communications*, vol. SAC-5, no. 5, pp. 879-889, Jun. 1987.

This Page Intentionally Left Blank

This Page Intentionally Left Blank

APPENDIX A: BASIC TRANSMISSION LOSS VERSUS DELAY SPREAD

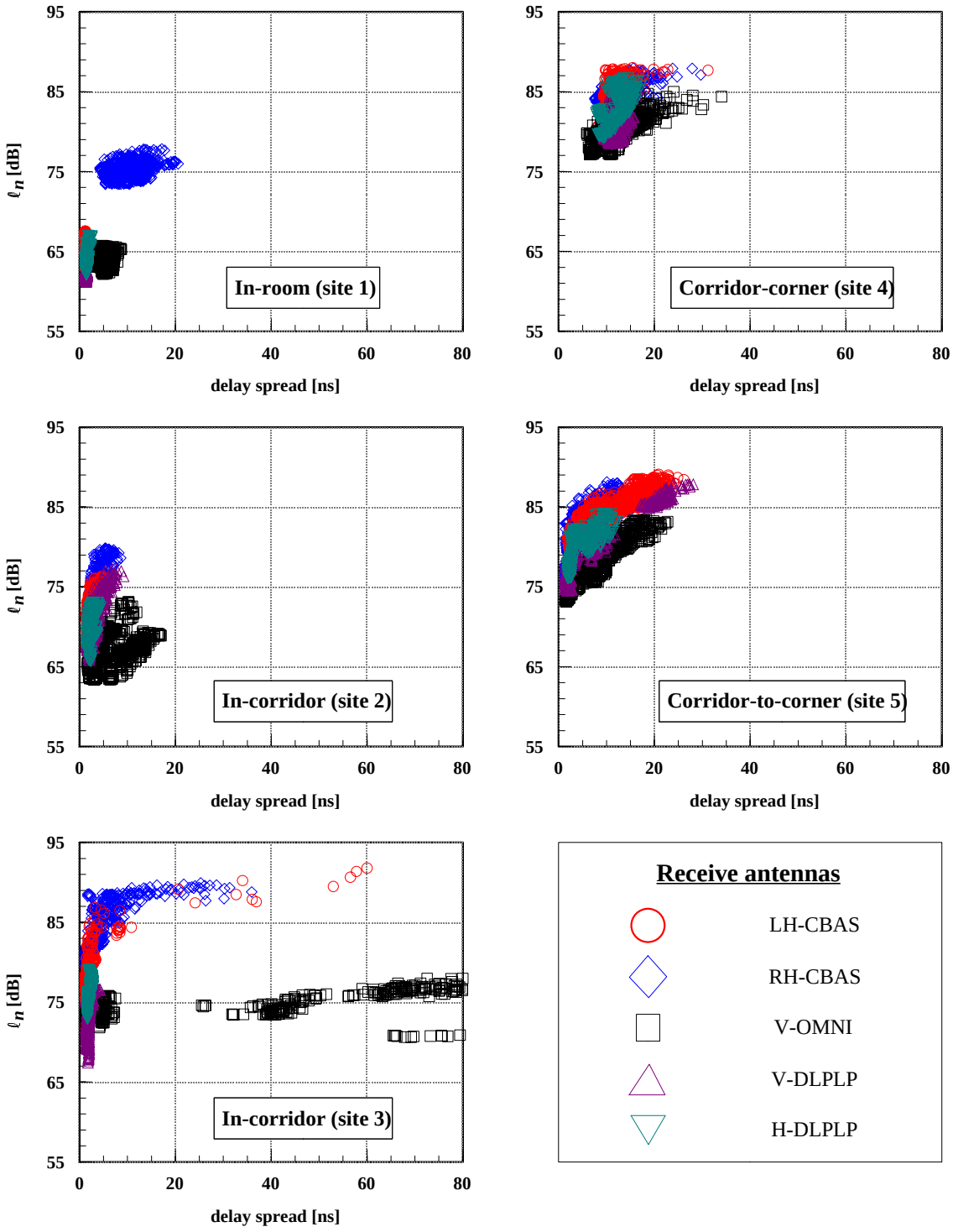

Figure A-1. Scatter plots of basic transmission loss versus delay spread of individual impulses for a LH-CBAS transmit antenna.

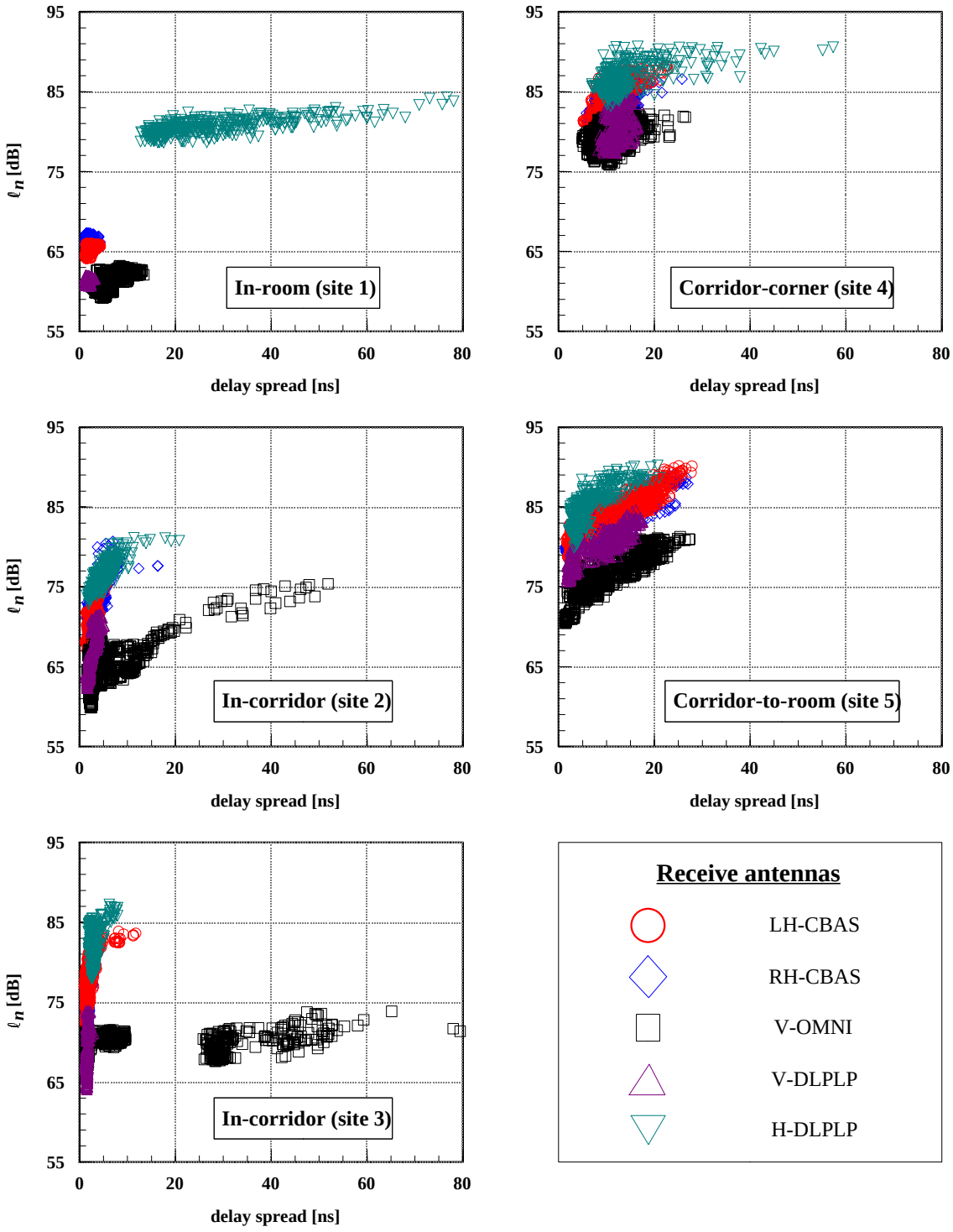

Figure A-2. Scatter plots of basic transmission loss versus delay spread of individual impulses for a V-LPLP transmit antenna.

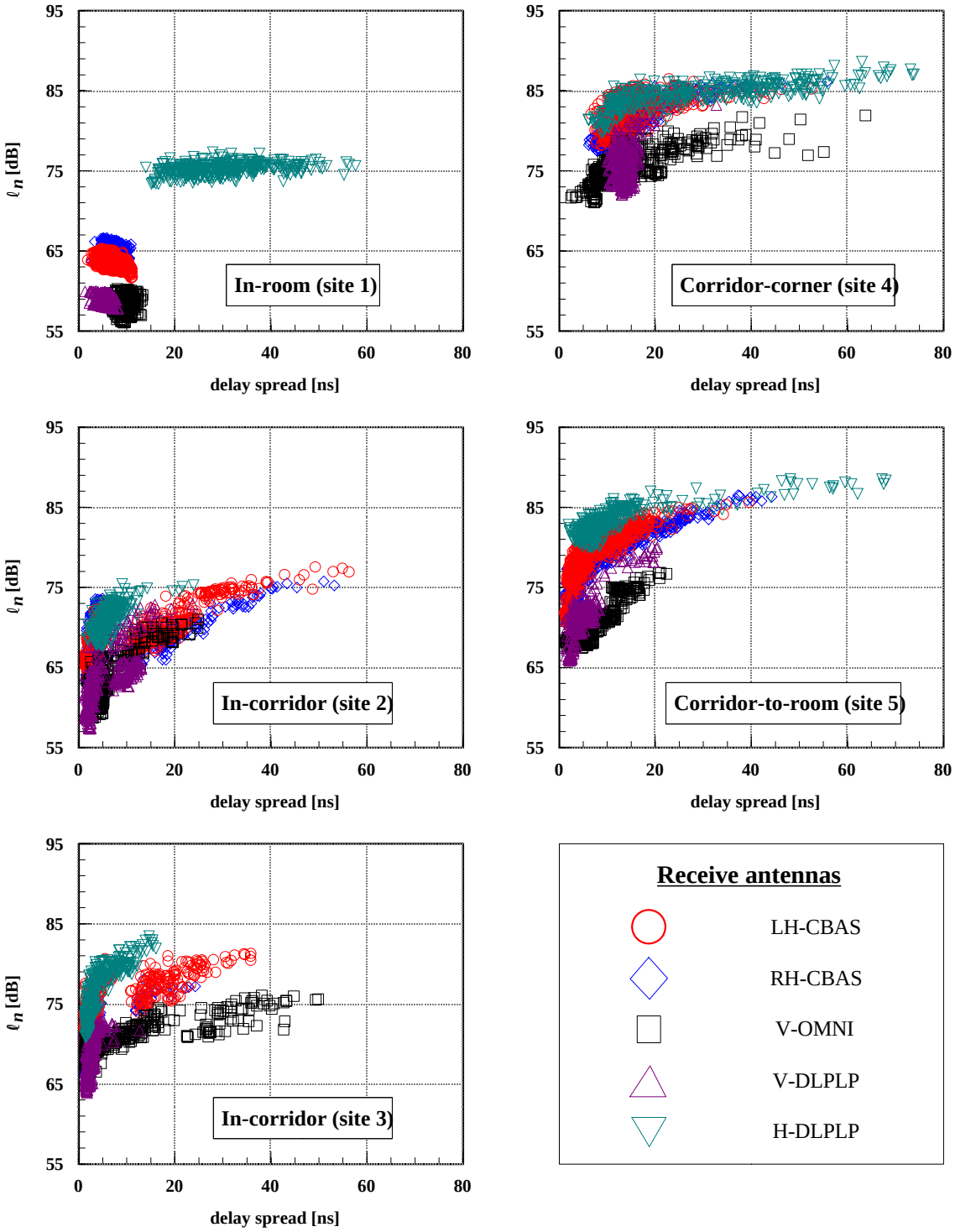

Figure A-3. Scatter plots of basic transmission loss versus delay spread of individual impulses for a V-OMNI transmit antenna.

This Page Intentionally Left Blank

This Page Intentionally Left Blank

APPENDIX B: MEASURED MEAN POWER DELAY PROFILES

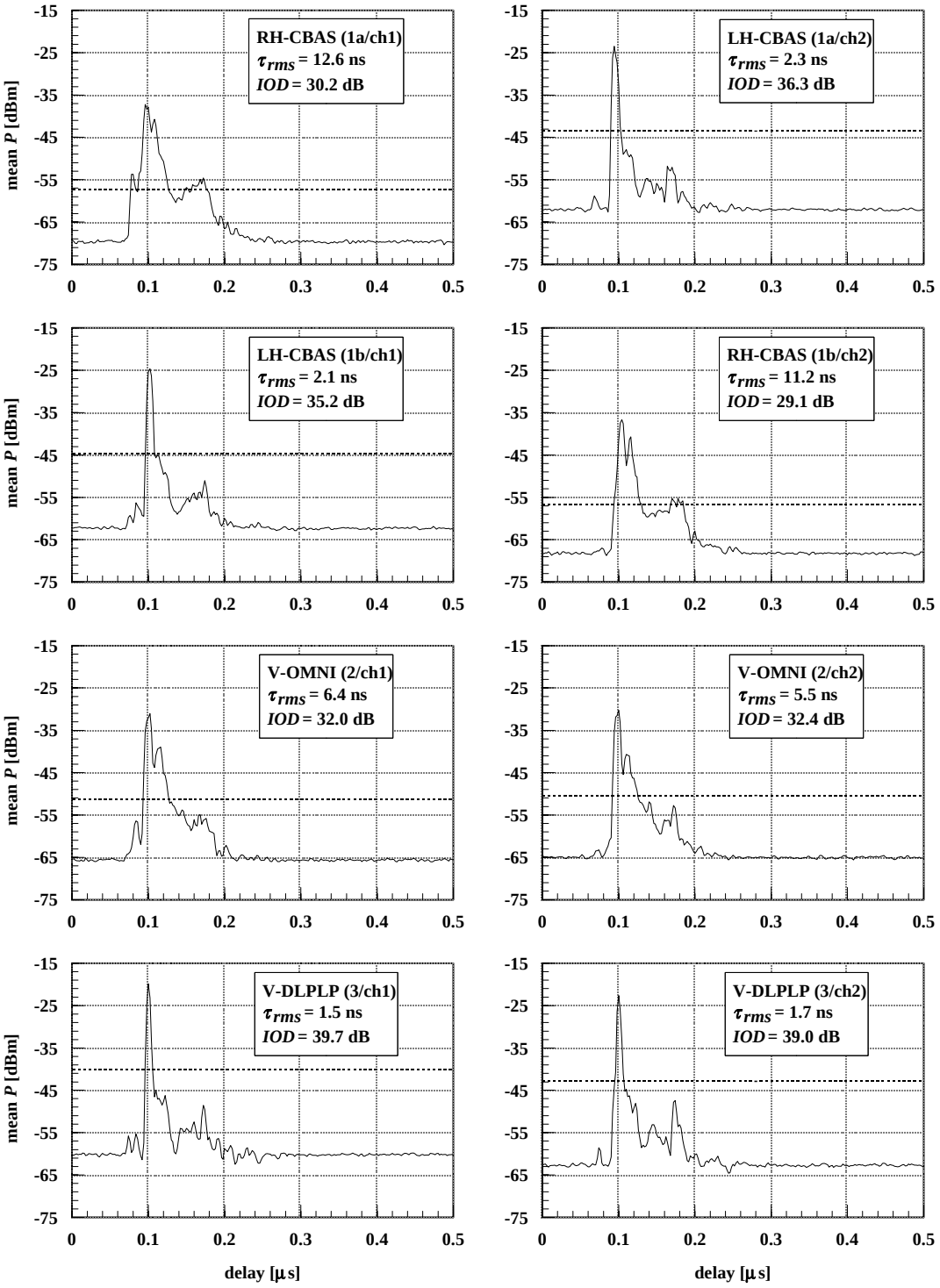

Figure B-1. Mean PDPs for in-room LOS scenario (site 1) with LH-CBAS transmit and various receive antennas. $d_{T\text{-}R}$ = 5.0 m, ψ = 180°, P_T = 6.2 dBm.

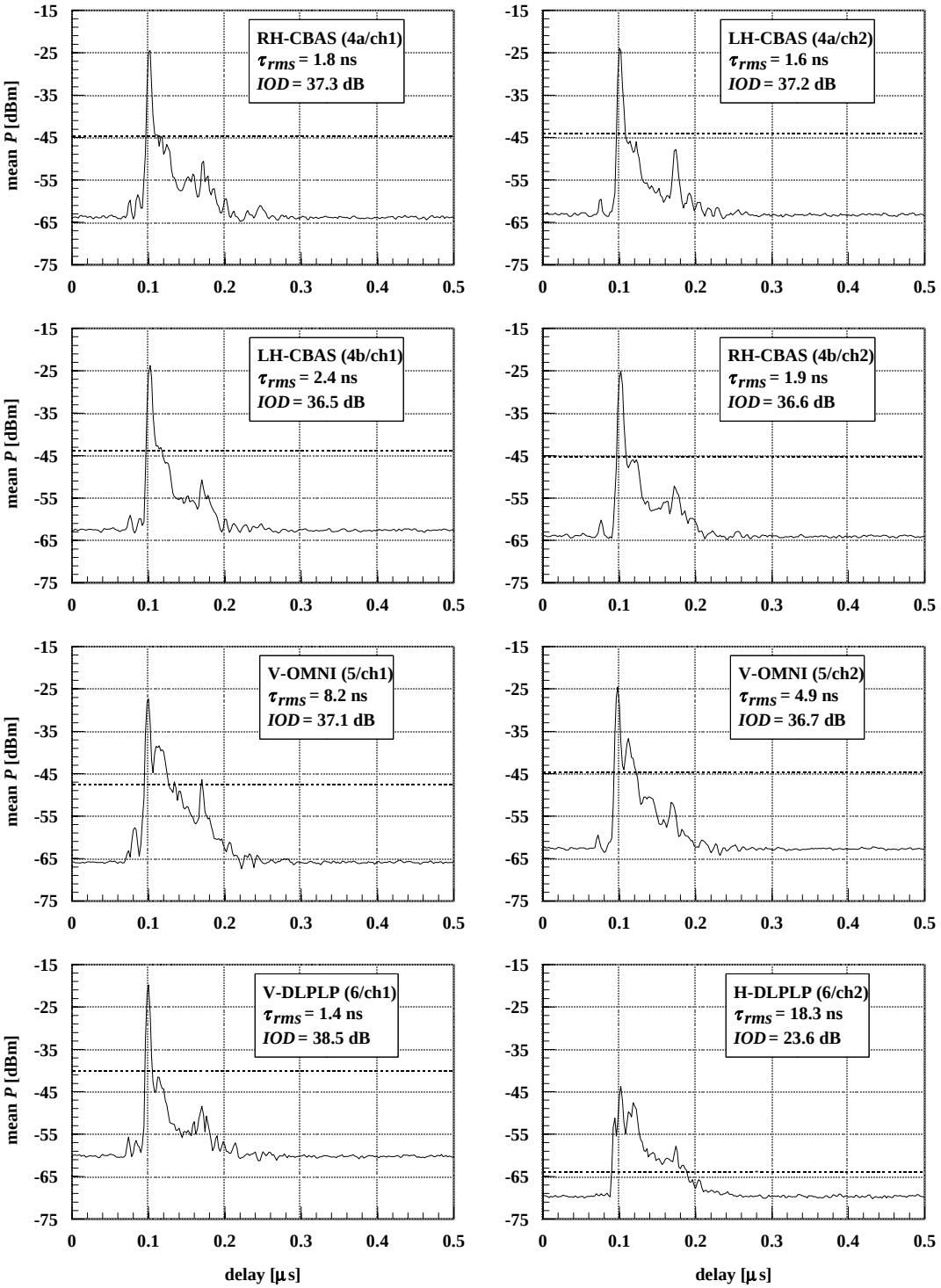

Figure B-2. Mean PDPs for in-room LOS scenario (site 1) with V-LPLP transmit antenna. $d_{T\text{-}R}$ = 5.0 m, ψ = 180°, P_T = 6.2 dBm.

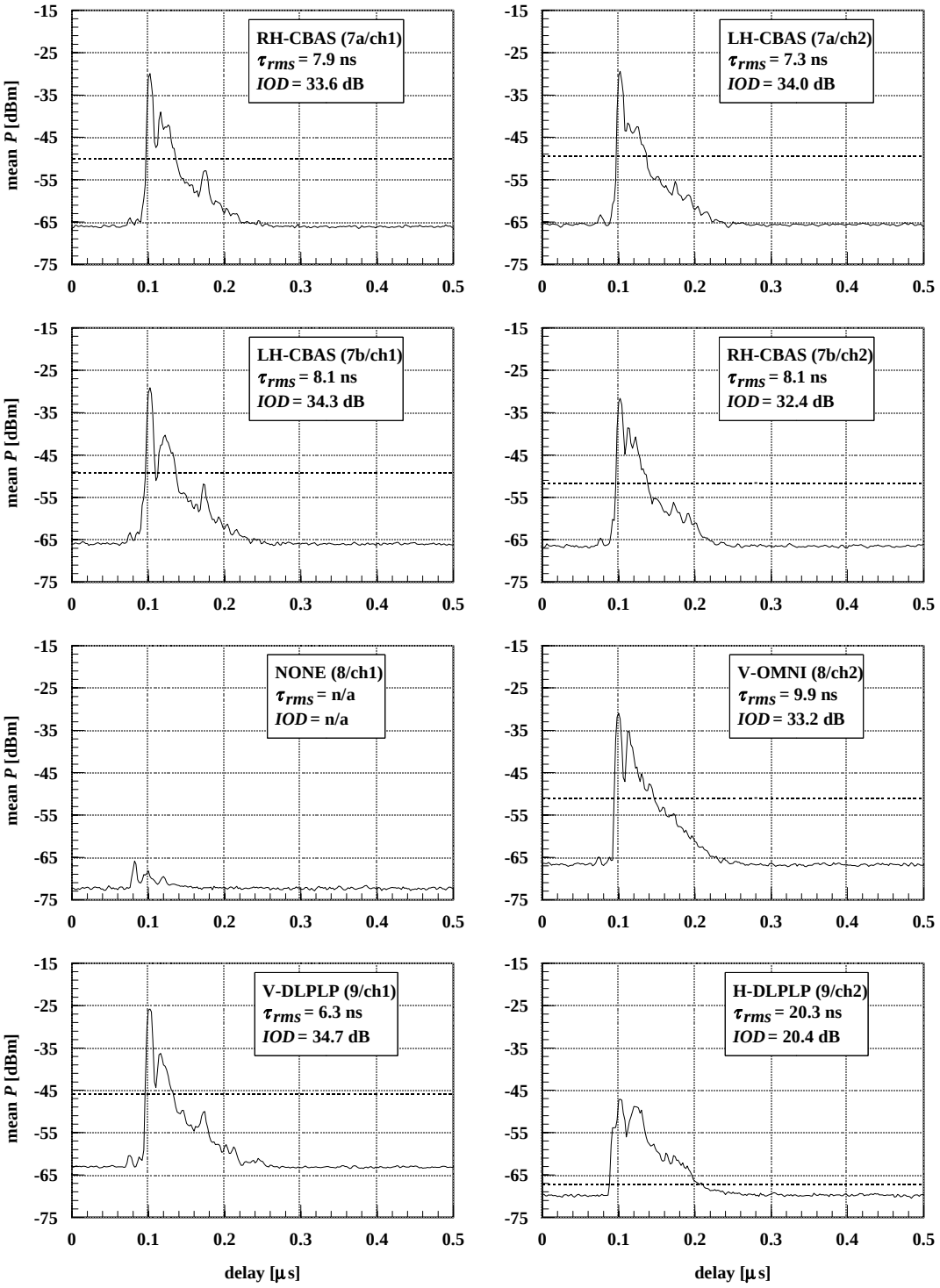

Figure B-3. Mean PDPs for in-room LOS scenario (site 1) with V-OMNI transmit antenna. $d_{T\text{-}R}$ = 5.0 m, ψ = 180°, P_T = 6.2 dBm.

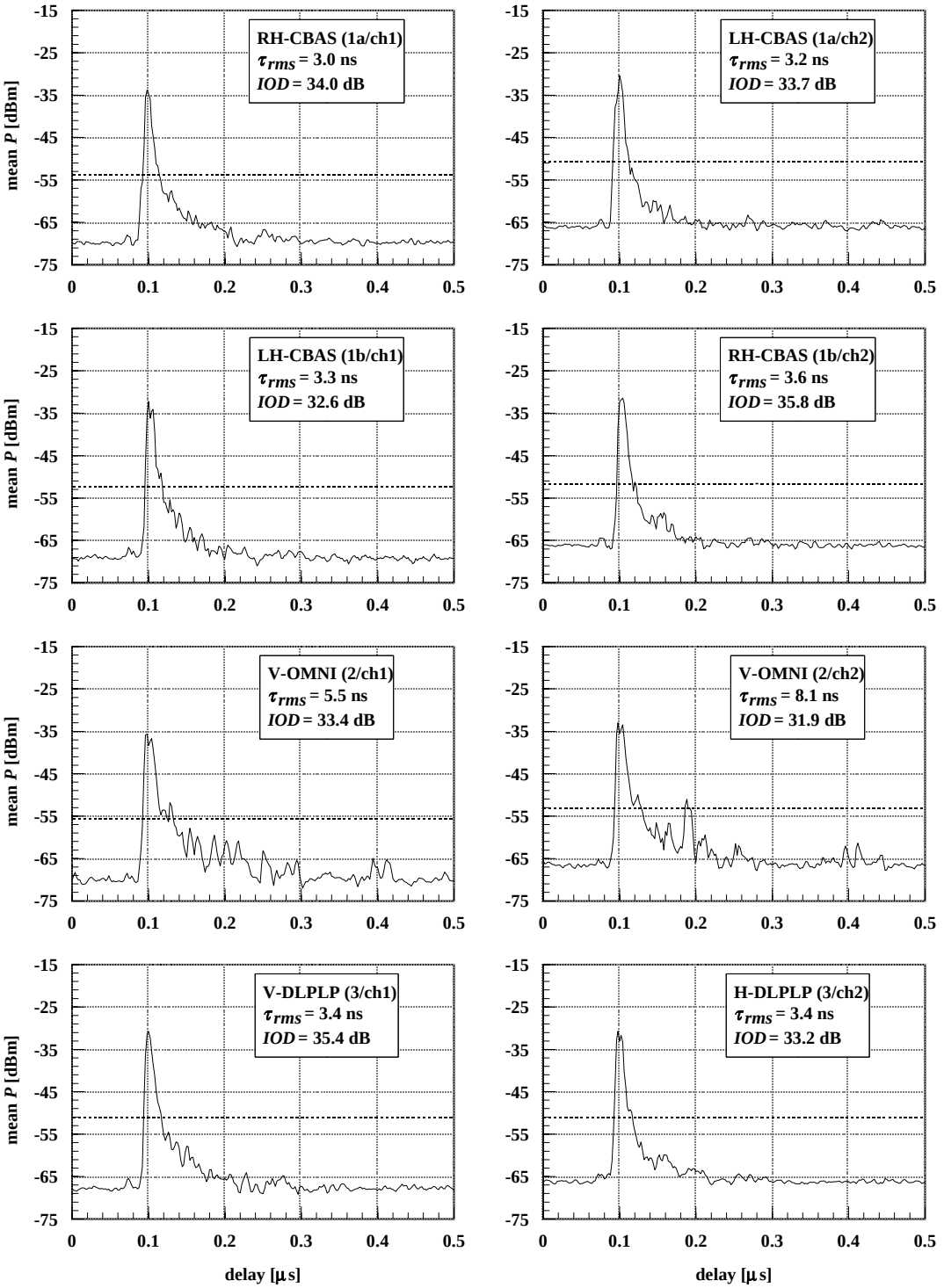

Figure B-4. Mean PDPs for in-corridor LOS scenario (site 2) with LH-CBAS transmit antenna. $d_{T\text{-}R}$ = 12.2 m, ψ = 180°, P_T = 6.2 dBm.

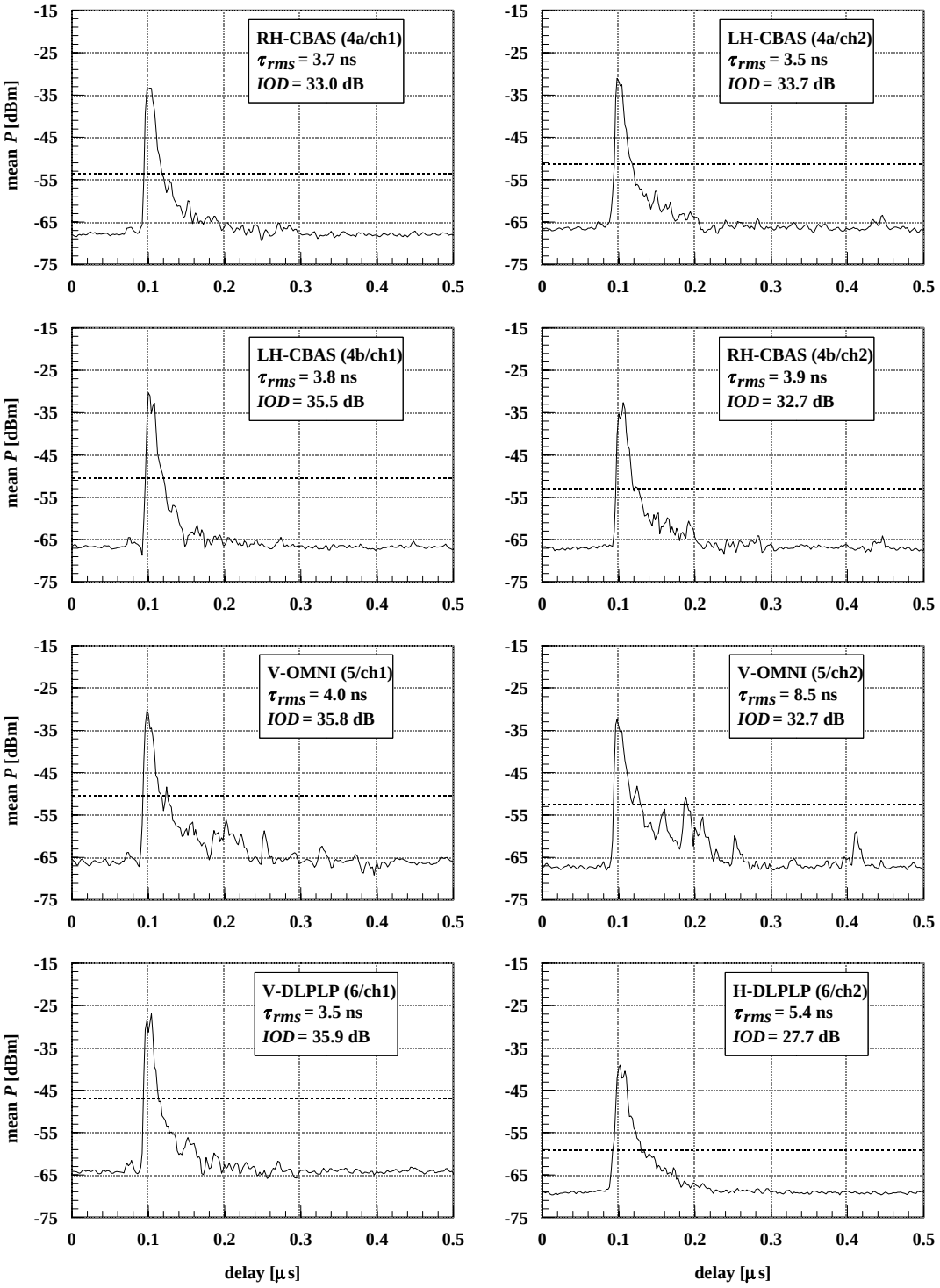

Figure B-5. Mean PDPs for in-corridor LOS scenario (site 2) with V-LPLP transmit antenna. $d_{T\text{-}R}$ = 12.2 m, ψ = 180°, P_T = 6.2 dBm.

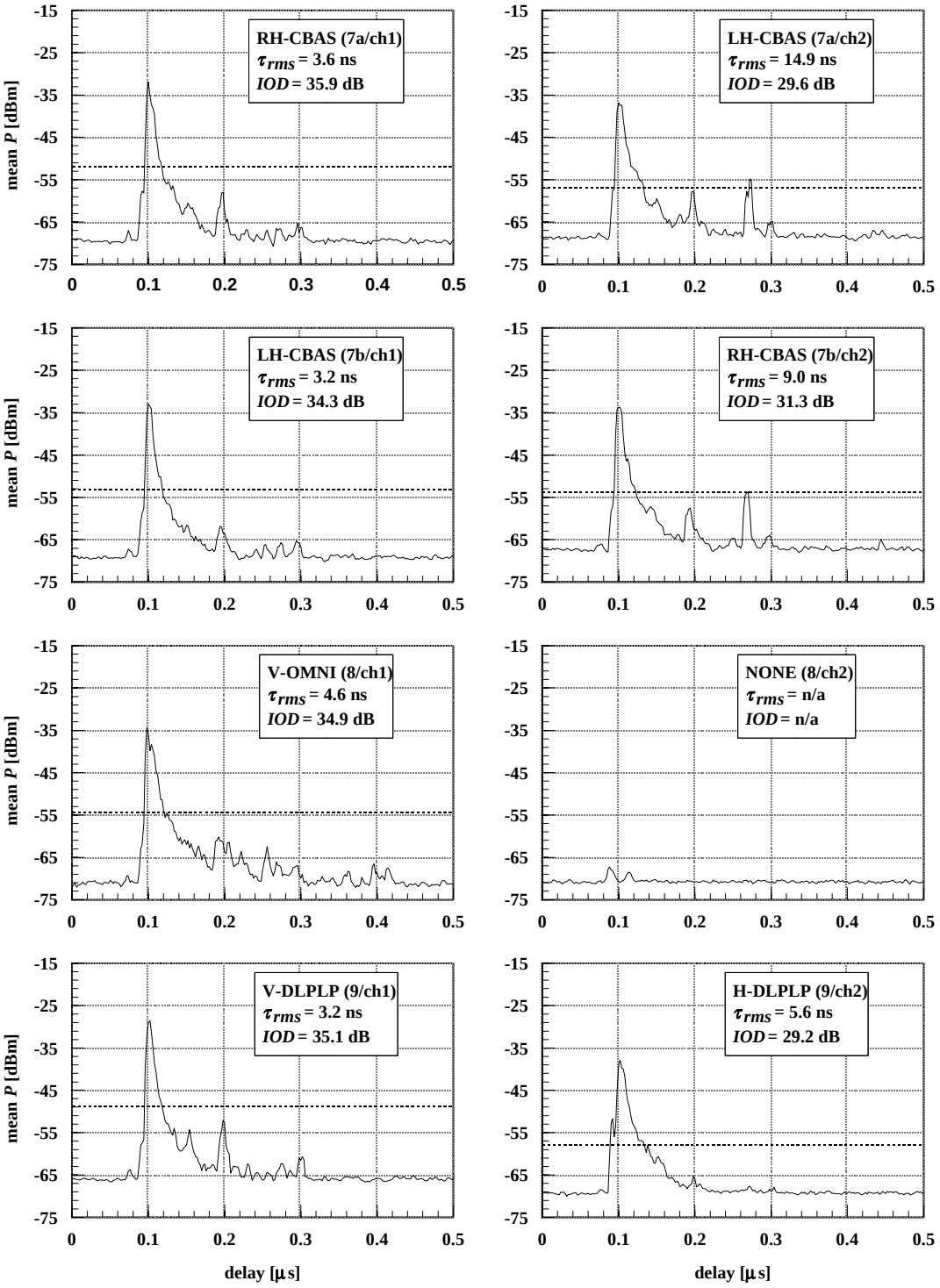

Figure B-6. Mean PDPs for in-corridor LOS scenario (site 2) with V-OMNI transmit antenna. $d_{T\text{-}R}$ = 12.2 m, ψ = 180°, P_T = 6.2 dBm.

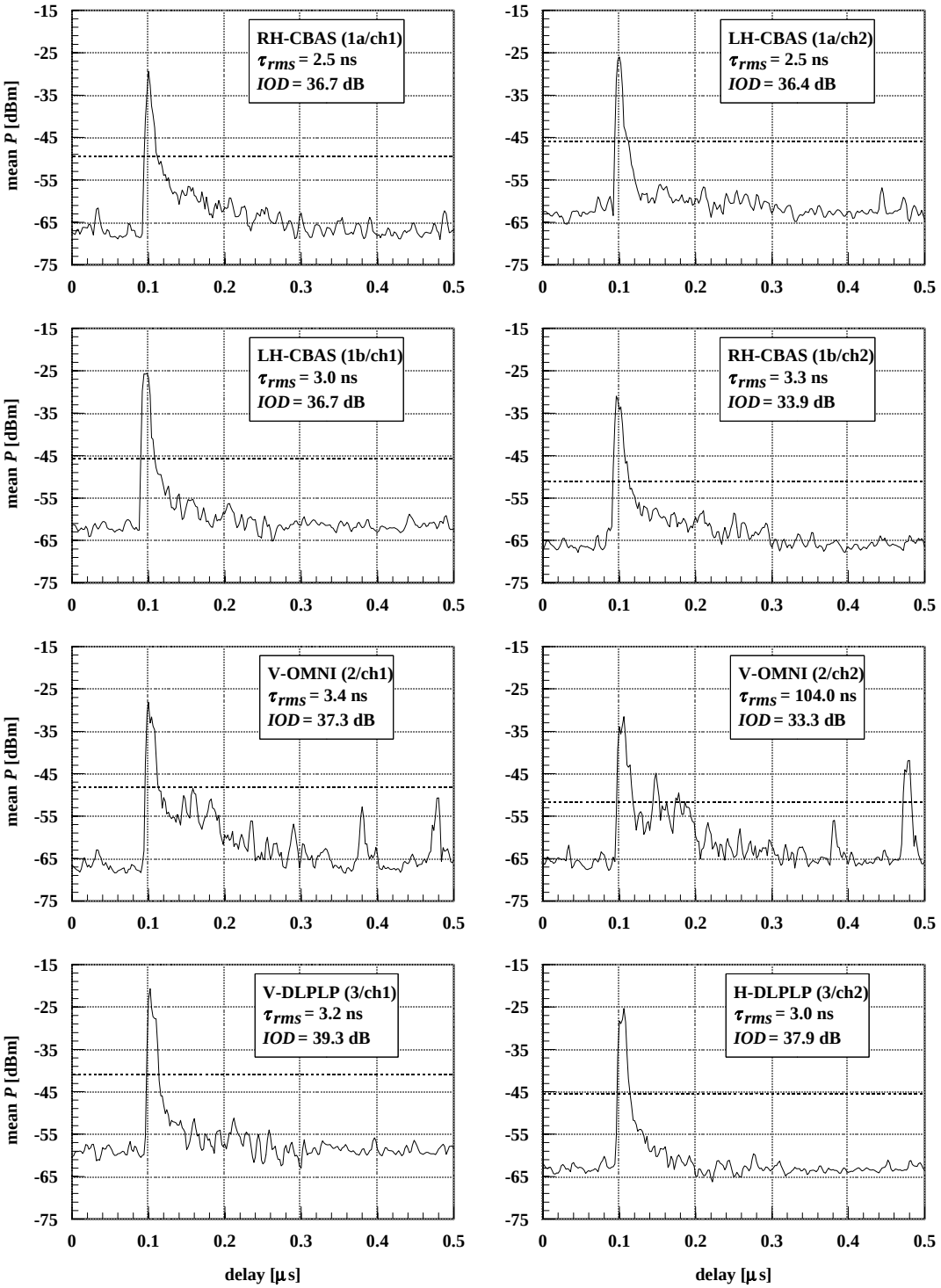

Figure B-7. Mean PDPs for in-corridor LOS scenario (site 3) with LH-CBAS transmit antenna. $d_{T\text{-}R}$ = 45.7 m, ψ = 180°, P_T = 17.0 dBm.

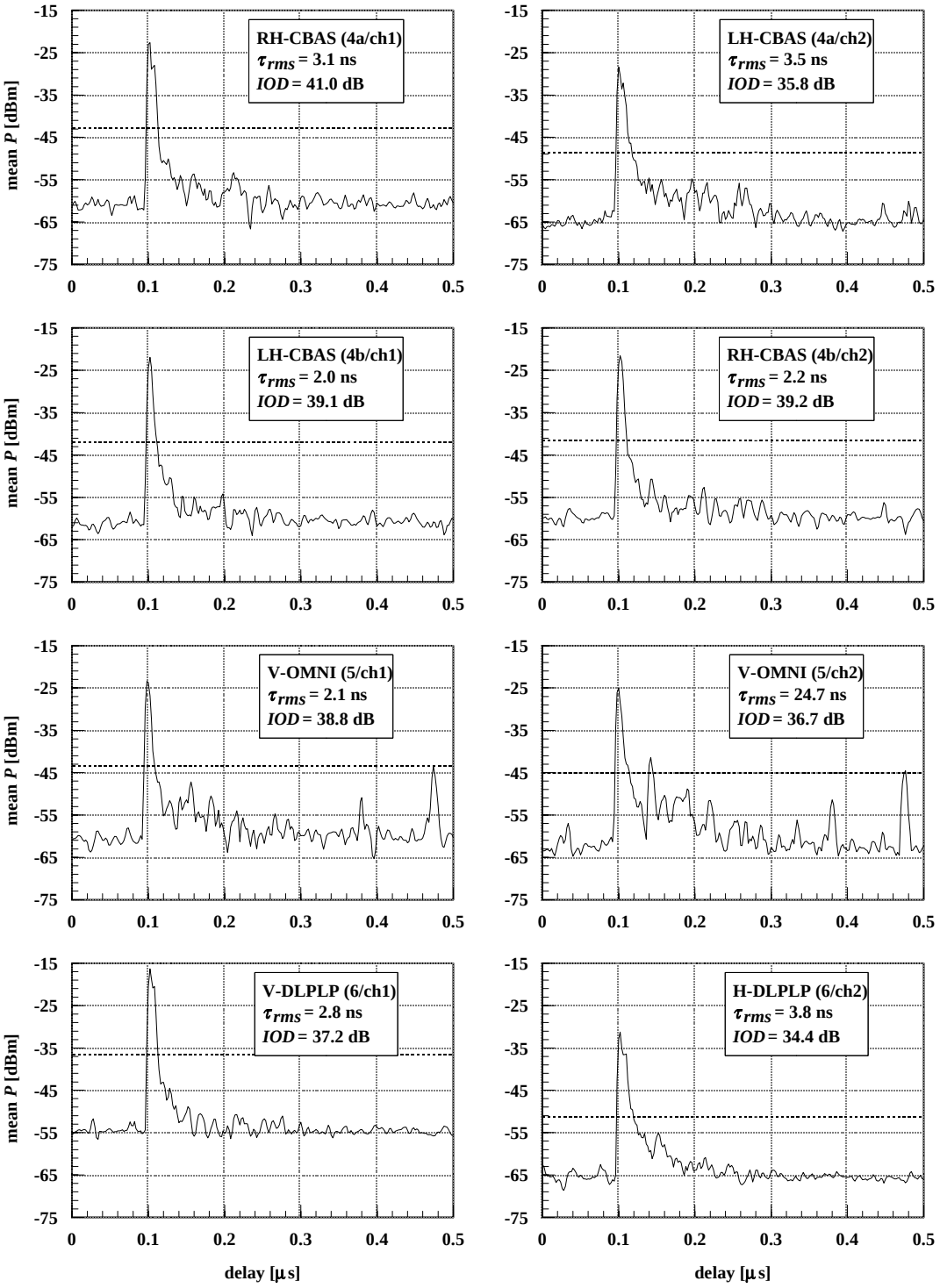

Figure B-8. Mean PDPs for in-corridor LOS scenario (site 3) with V-LPLP transmit antenna. $d_{T\text{-}R}$ = 45.7 m, ψ = 180°, P_T = 17.0 dBm.

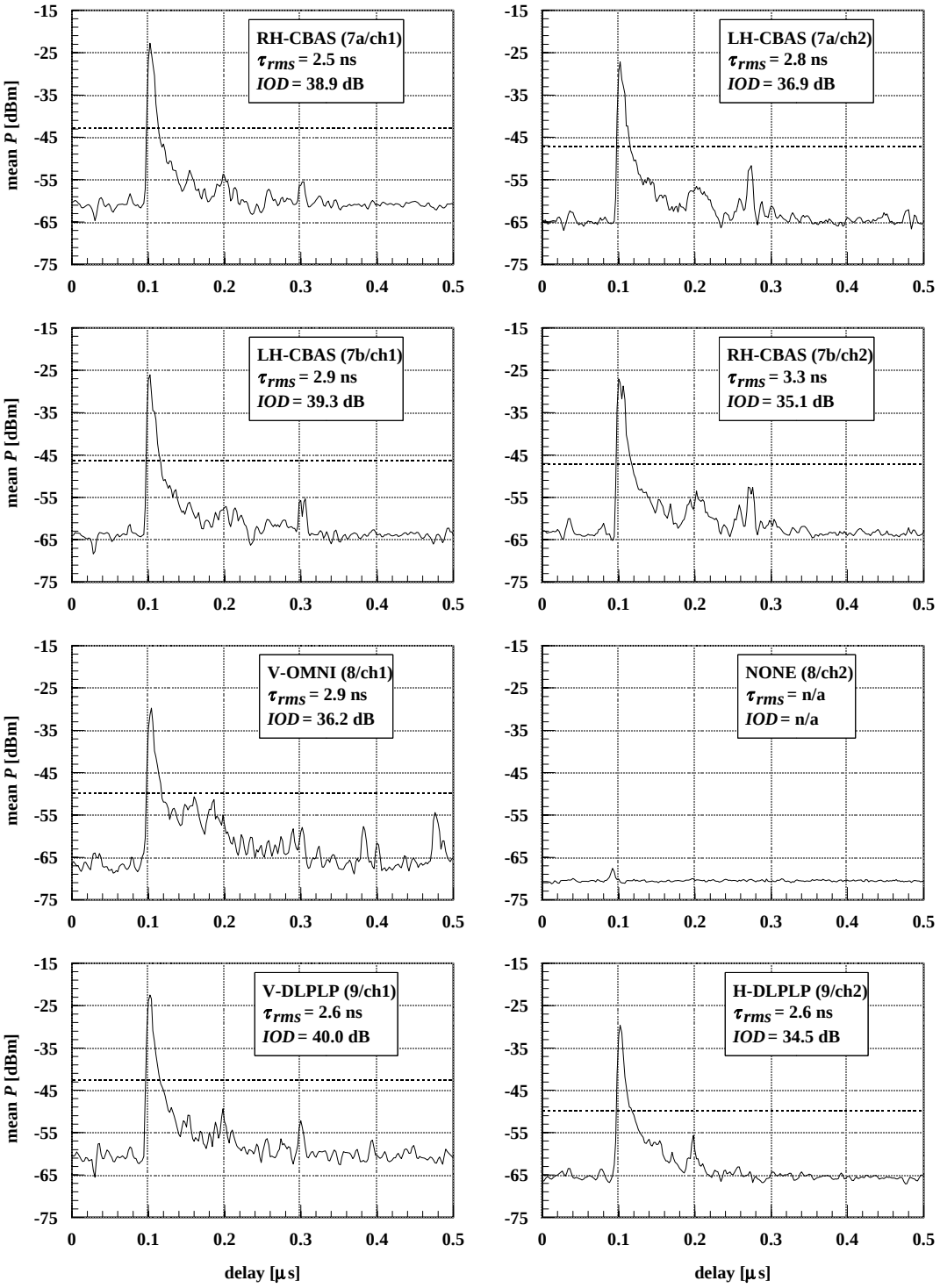

Figure B-9. Mean PDPs for in-corridor LOS scenario (site 3) with V-OMNI transmit antenna. $d_{T\text{-}R}$ = 45.7 m, ψ = 180°, P_T = 17.0 dBm.

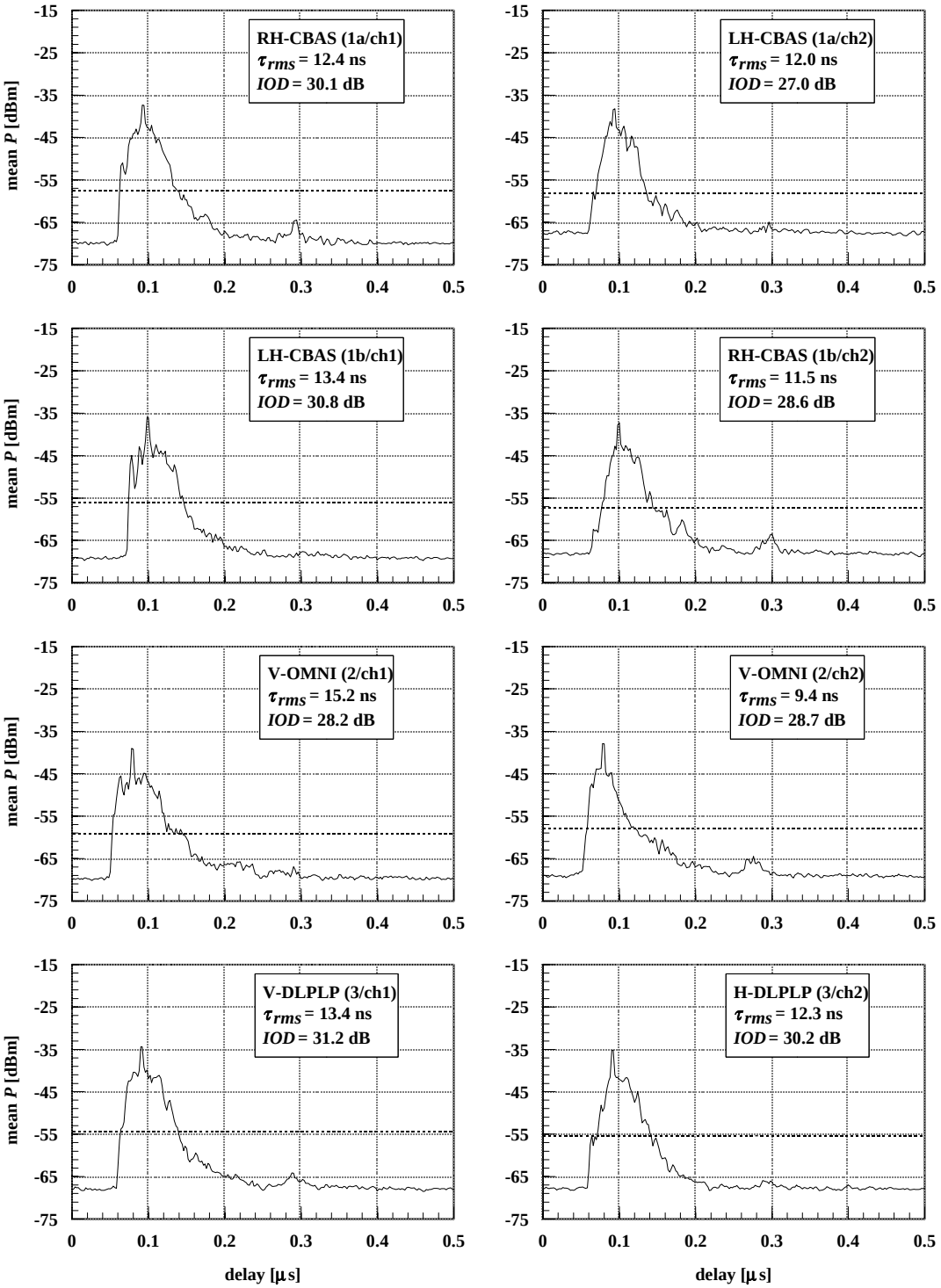

Figure B-10. Mean PDPs for corridor-corner OBS scenario (site 4) with LH-CBAS transmit antenna. $d_{T\text{-}R}$ = 8.3 m, ψ = 90°, P_T = 16.2 dBm.

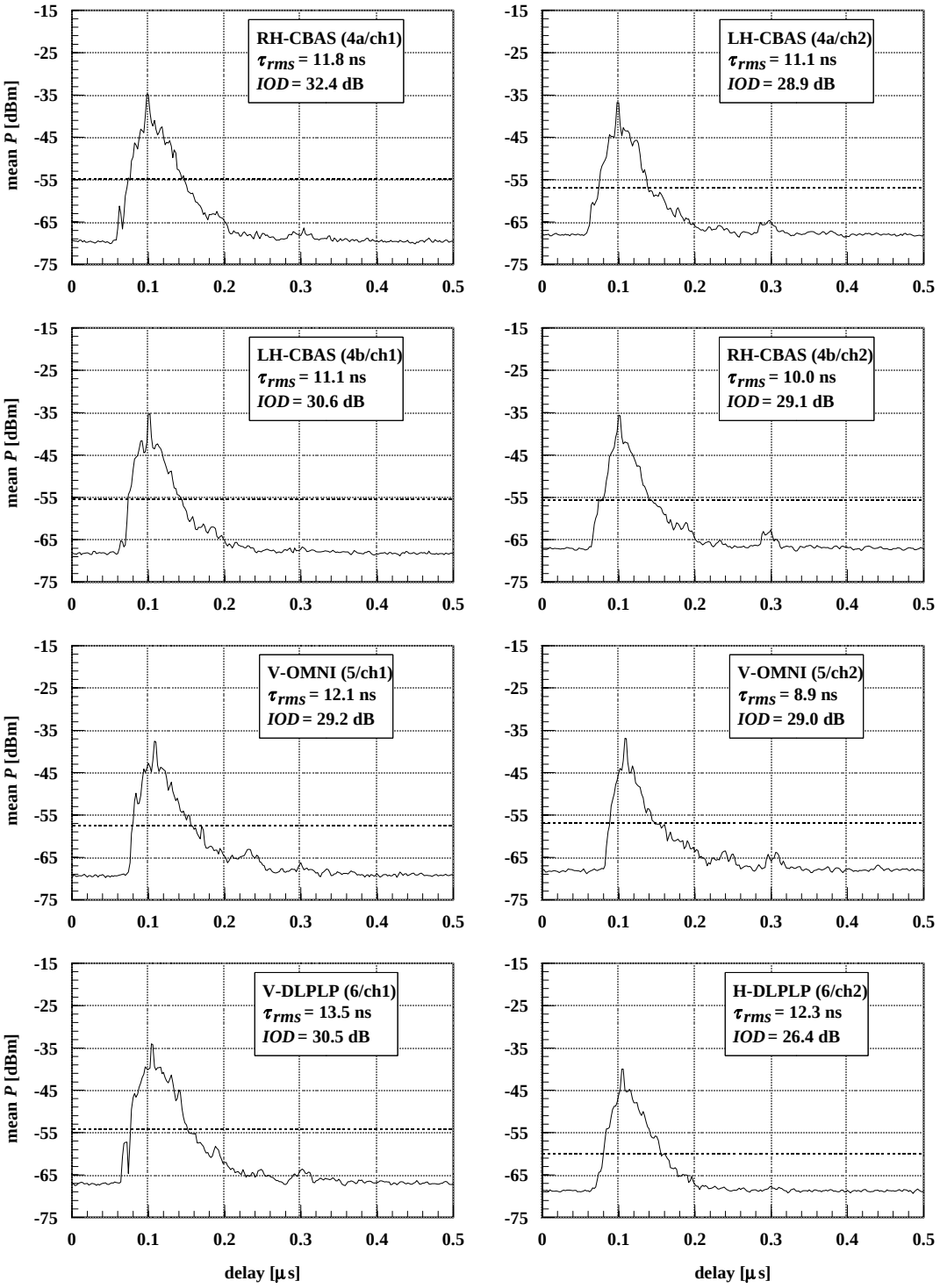

Figure B-11. Mean PDPs for corridor-corner OBS scenario (site 4) with V-LPLP transmit antenna. $d_{T\text{-}R}$ = 8.3 m, ψ = 90°, P_T = 16.2 dBm.

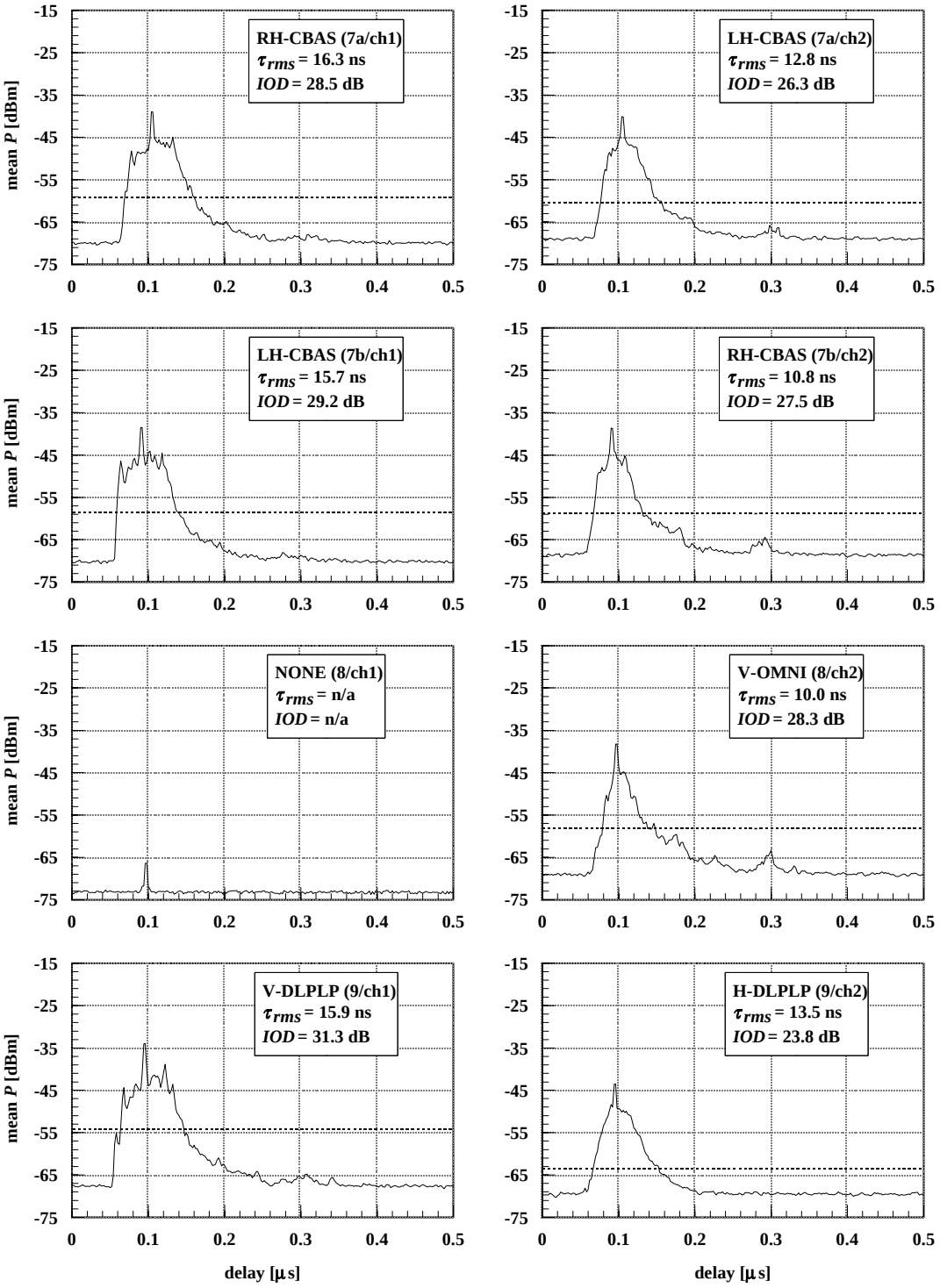

Figure B-12. Mean PDPs for corridor-corner OBS scenario (site 4) with V-OMNI transmit antenna. $d_{T\text{-}R}$ = 8.3 m, ψ = 90°, P_T = 16.2 dBm.

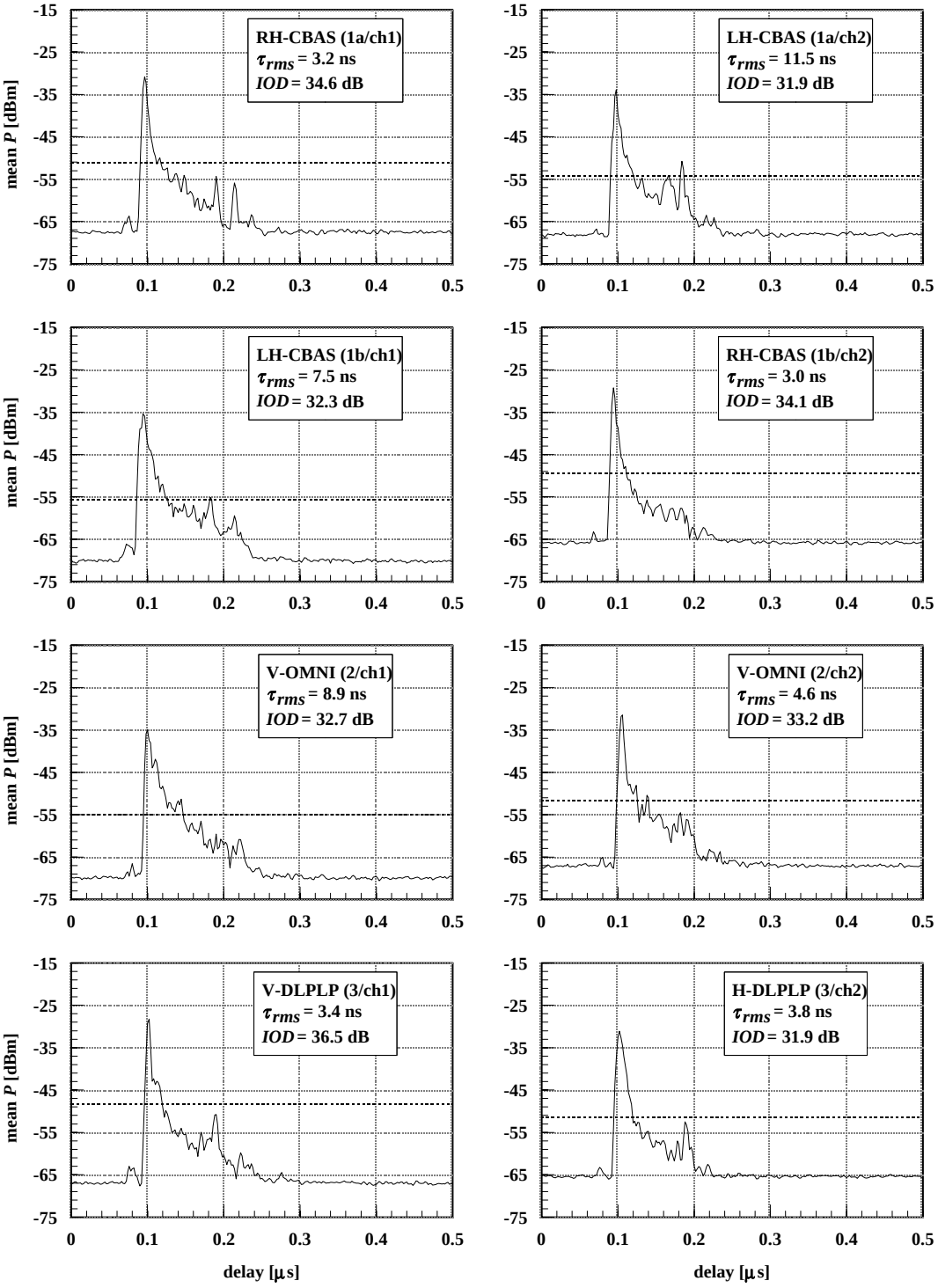

Figure B-13. Mean PDPs for corridor-to-room OBS scenario (site 5) with LH-CBAS transmit antenna. $d_{T\text{-}R}$ = 13.7 m, ψ = 152.8°, P_T = 16.2 dBm.

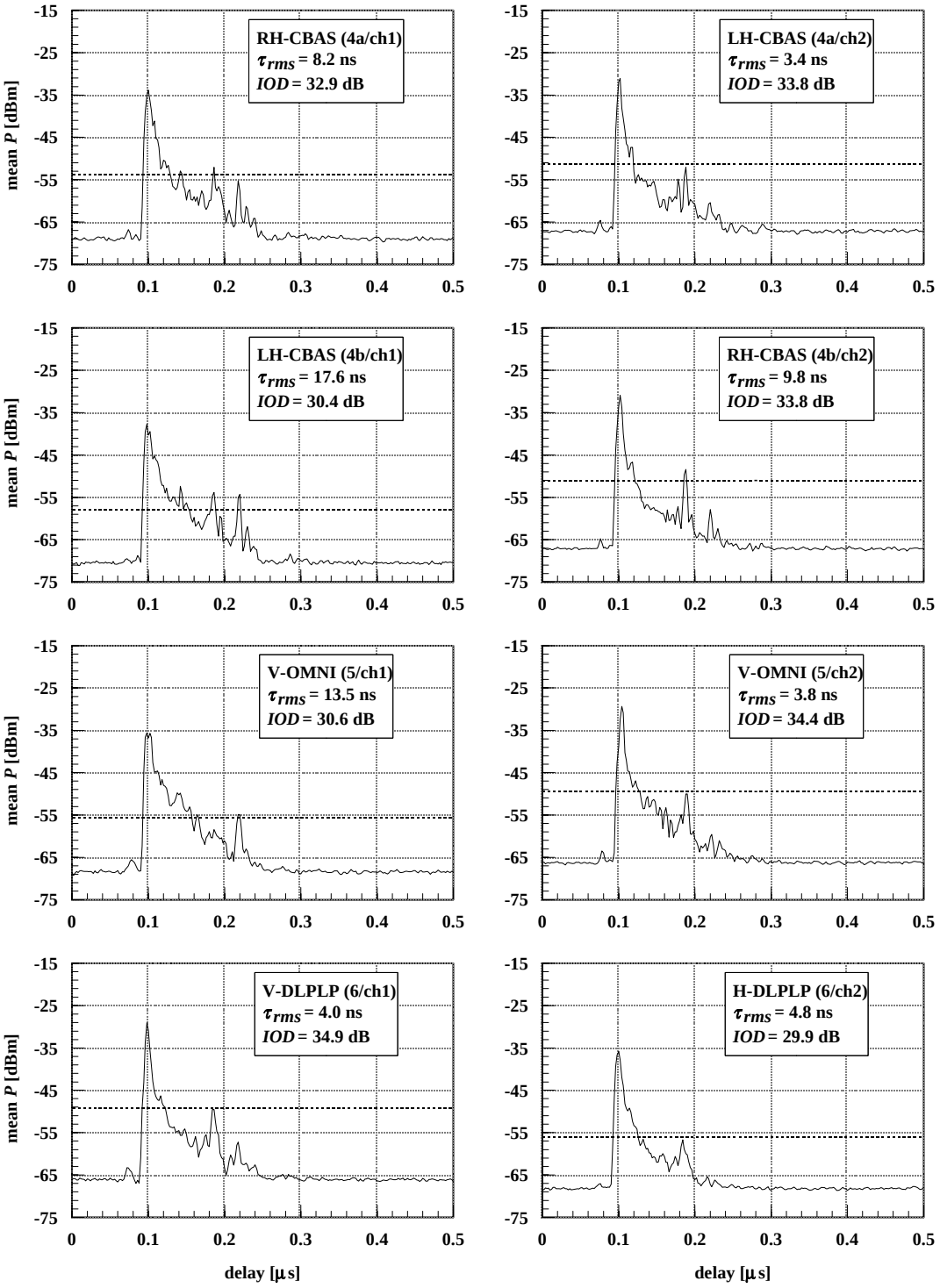

Figure B-14. Mean PDPs for corridor-to-room OBS scenario (site 5) with V-LPLP transmit antenna. $d_{T\text{-}R}$ = 13.7 m, ψ = 152.8°, P_T = 16.2 dBm.

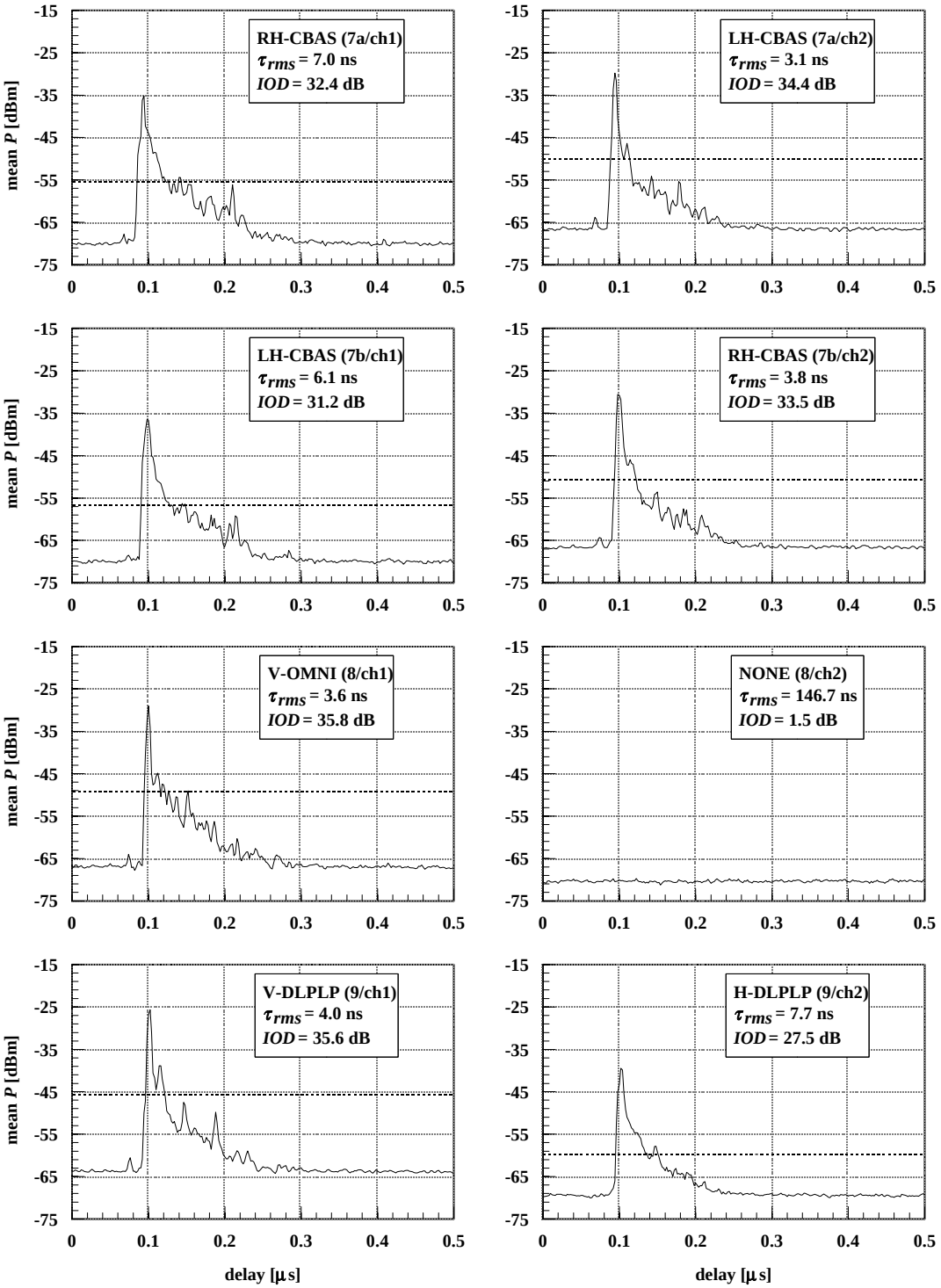

Figure B-15. Mean PDPs for corridor-to-room OBS scenario (site 5) with V-OMNI transmit antenna. $d_{T\text{-}R}$ = 13.7 m, ψ = 152.8°, P_T = 16.2 dBm.

This Page Intentionally Left Blank

This Page Intentionally Left Blank

APPENDIX C: SYSTEM COMPONENT DESCRIPTION

The acronyms in front of each component specification are used in Figures 3 and 4.

C.1. Transmitter Component Specification

A1: Low noise amplifier, frequency range: 1-2 GHz, 35-dB gain
A2: Low noise amplifier, frequency range: 4-8 GHz, 26-dB gain, 1-dB compression at 23 dBm, 6-dB N.F.
F1: Band pass filter, 5-pole Chebychev, 0.35-dB insertion loss, 3-dB bandwidth: 1000 MHz
F2: Band pass filter, 5-pole Chebychev, 0.26-dB insertion loss, 3-dB bandwidth: 1000 MHz
LO1: Local oscillator, 1.5 GHz, +7-dBm output power
LO2: Local oscillator, 4.3 GHz, +10-dBm output power
M1: Double balanced mixer
M2: Double balanced mixer, 6.5-dB conversion loss, 1-dB compression at +5 dBm
P1: Attenuator, 3 dB
P2: Attenuator, 10 dB
P3: Attenuator, 3 dB
P4: Attenuator, 10 dB

C.2. Receiver Component Specifications

A3: Low noise amplifier, 4-8 GHz, 37-dB gain, 1-dB compression at 10 dBm, 1.8-dB N.F.
A4, A7: Medium power amplifier, 10-2000 MHz, 20-dB gain, 1-dB compression at +16 dBm, 7 dB N.F.
A5, A8: Low power amplifier, 0.05-500 MHz, 20-dB gain min., power out 1-dB compression at +9 dBm, 5.3 dB N.F
A6: Low noise amplifier, 4-8 GHz, 34-dB gain, 1-dB compression at +10 dBm, 1.8-dB N.F.
F3, F6: Bandpass filter, 5-pole Chebychev, 0.26-dB insertion loss, 3-dB bandwidth: 1000 MHz
F4, F7: Bandpass filter, 6-pole Chebychev, 3-dB bandwidth: 500 MHz
F5, F8: Low pass filter, DC-520-MHz passband, insertion loss < 1 dB, 3-dB loss at 570 MHz
LO3: Local oscillator, 4.3 GHz, +10-dBm output power
LO4: Local oscillator, 1.75 GHz, +7-dBm output power
M3, M5: Double balance mixer, 8-dB conversion loss, 1-dB compression at +6 dBm
M4, M6: Double balance mixer, 7.5-dB conversion loss, +1-dBm RF max power
P5: Attenuator, 3 dB
P6: Attenuator, 10 dB
P7, P10: Attenuator, 3 dB
P8, P11: Attenuator, 10 dB
P9: Attenuator, 9 dB